Numerical Simulation of Extreme Wave Loading

on Deep-water SPAR Platforms using the SPH Method

by

Ivan Gan Wei Ren

16522

Dissertation submitted in partial fulfilment of
the requirements for the
Bachelors of Engineering (Hons)
Mechanical Engineering

Jan 2016

Universiti Teknologi PETRONAS
Bandar Seri Iskandar
32610 Tronoh
Perak Darul Ridzuan

CERTIFICATION OF APPROVAL

Numerical Simulation of Extreme Wave Loading

on Deep-water SPAR Platforms using the SPH Method

By

IVAN GAN WEI REN
16522

A project dissertation submitted to the
Mechanical Engineering Programme
Universiti Teknologi PETRONAS
in partial fulfilment of the requirement for the
BACHELOR OF ENGINEERING (Hons)
(MECHANICAL)

Approved by,

_____

(Dr. William Pao King Soon)

UNIVERSITI TEKNOLOGI PETRONAS
TRONOH, PERAK
January 2016

CERTIFICATION OF ORIGINALITY

This is to certify that I am responsible for the work submitted in this project, that the original work is my own except as specified in the references and acknowledgements, and that the original work contained herein have not been undertaken or done by unspecified sources or persons.

_____

IVAN GAN WEI REN

ACKNOWLEDGEMENT

I would like to take this chance to express my most heartfelt gratitude to all the people and institutions that have aided in my Final Year Project journey.

First of all, I would like to thank my direct supervisor, Dr. William Pao King Soon of Mechanical Engineering Department, Universiti Teknologi PETRONAS. Thank you for your most passionate and straightforward way of teaching and educating your pupils. Each and every lesson I will remember. I would also like to thank all my friends and colleagues who have supported and gave me guidance in each leg of this journey.

Last but not least, I acknowledge with a deep sense of reverence, my gratitude towards my parents and family members, who has always supported me morally and motivated me to made headway in the project.

Abstract

Real-life experimental models take a lot of time and monetary resources to construct and run. These set-ups are expensive and inflexible, requiring a new model to be built for differing conditions. The oil and gas industry requires fast and accurate testing of certain models such as production platform, e.g. SPAR Platforms.

This research attempts to construct a simulation model that replicates the wave reactions of deep-water floating SPAR Platforms. This study also aims to build a clear correlation between varying wave amplitude, water depth and wave frequency to the wave impact pressure of deep-water SPARs.

This study shall be carried out first by simulating a few validation examples using the Smoothed Particle Hydrodynamics Model. Once validation has been completed, the simulation model for the SPAR Platform shall be constructed using the SPH model. The simulation results are then processed using post-processing routines such as ParaView and Matlab to predict the flow of the fluid and the angular pitch of the SPAR Platform.

At the end of the simulations, the wave impact pressures and fluid motion can be accurately predicted using the Smoothed Particle Hydrodynamics model constructed. This would save oil and gas companies time and money by not having to construct real-time experimental set-ups to test new rigs and production platforms.

Table of Contents

Chapter 1 Introduction 1
1.1 Background of Study 1
1.2 Problem Statement 2
1.3 Objectives and Scope of Study 3
1.3.1 Objectives 3
1.3.2 Scope of study 3
Chapter 2 Literature Review 4
2.1 Offshore floating structures 4
2.2 Types of offshore floating structures 4
2.2.1 Floating Production, Storage and Offloading Vessels (FPSO) 4
2.2.2 Semi-submersibles 5
2.2.3 SPAR Platforms 5
2.3 Wave loading on offshore floating structures 6
2.4 Software-aided simulation methods 6
2.4.1 Smoothed Particle Hydrodynamics (SPH) Method 7
2.4.2 Governing Equations 7
2.4.3 Weakly Compressible SPH algorithm 8
2.4.4 Kernel Function Approximation in SPH 8
2.4.5 Artificial Viscosity 9
2.5 Effect of Relative Wave Height and Air Gap to the Wave Impact Pressure 9
2.5.1 Effect of Wave Height on the Wave Impact Load to the Platforms 10
Chapter 3 Methodology 12
3.1 FYP Gantt Chart & Project Key Milestones 12
3.2 FYP Flowchart 13
3.3 Validation Example 1 : Dam Break with Trapezoid Obstacle 14
3.3.1 Initial and Boundary Conditions 14

3.4 Validation Example 2 : Dam Break Flow 16
3.5 Development of Simulation Model 19
3.5.1 Model 1 (Sloped Shoreline) 19
Chapter 4 Results & Discussion 21
4.1 Validation Results 21
4.1.1 Validation Example 1 (Dam Break with Trapezoid Obstacle) 21
4.1.2 Validation Example 2 (Dam Break Flow) 25
4.2 Simulation of SPAR Platform on a Beach or Sloped Seabed 32
4.3 Effect of Varying Water Depth on Angular Pitch of SPAR 35
4.4 Effect of Varying Wave Frequency on Angular Pitch of SPAR 39
4.5 Effect of Varying Wave Amplitude on Angular Pitch of SPAR 42
Chapter 5 Conclusions & Recommendations 45
5.1 Conclusions 45
5.2 Recommendations 45
Chapter 6 References 46

List of Equations

EQUATION 1 NAVIER STOKES EQUATIONS IN WCSPH 8
EQUATION 2 EQUATION OF STATE IN WCSPH 8
EQUATION 3 ARTIFICIAL VISCOSITY 9

List of Tables

TABLE 1 PARAMETERS FOR SIMULATION 34
TABLE 2 REFERENCE LINE CORRESPONDING TO WATER DEPTH 36
TABLE 3 WAVE FREQUENCY VARIATIONS 39
TABLE 4 WAVE AMPLITUDE VARIATIONS 42

List of Figures

FIGURE 1 TYPES OF OFFSHORE STRUCTURES 1
FIGURE 2 SEMI SUBMERSIBLE PLATFORM 5
FIGURE 3 TYPICAL SPAR PLATFORM BUILD 5
FIGURE 4 COMPARISON OF NORMALIZED PEAK PRESSURE WITH EXPERIMENTS 9
FIGURE 5 IMPACT PEAK PRESSURE P_P/PGD WITH H/D AND S/D (WANG, 1996) 10
FIGURE 6 PEAK FORCE VERSUS WAVE HEIGHT [FX = HORIZONTAL LOAD, FZ = VERTICAL LOAD] (LUBEENA & GUPTA, 2013) 10
FIGURE 7 HORIZONTAL FORCE FX/PGD2WITH H/D AND S/D (WANG, 1996) 11
FIGURE 8 VERTICAL FORCE FY/PGD2 WITH H/D AND S/D (WANG, 1996) 11
FIGURE 9 THE EXPERIMENTAL SET-UP OF DAM BREAK MECHANISM (OZMEN-CAGATAY & KOCAMAN, 2011) 14
FIGURE 10 THE COMPUTED SURFACE PROFILES AT DIFFERENT POINTS OF TIME (OZMEN-CAGATAY & KOCAMAN, 2011) 15
FIGURE 11 EXPERIMENTAL SET-UP (PABLO A. CARON, 2015) 16
FIGURE 12 DAM BREAK AT T=0.1 SEC 16
FIGURE 13 DAM BREAK AT T=0.2 SEC 17
FIGURE 14 DAM BREAK AT T=0.3 SEC 17
FIGURE 15 DAM BREAK AT T=0.4 SEC 17
FIGURE 16 DAM BREAK AT T=0.5 SEC 17
FIGURE 17 DAM BREAK AT T=0.6 SEC 17
FIGURE 18 DAM BREAK AT T=0.7 SEC 17
FIGURE 19 DAM BREAK AT T=0.8 SEC 18
FIGURE 20 DAM BREAK AT T=0.9 SEC 18
FIGURE 21 DAM BREAK AT T=1.0 SEC 18
FIGURE 22 PROPOSED MODEL FOR SPAR PLATFORM SIMULATION 19
FIGURE 23 GENERATED SOLUTION DOMAIN FOR SPAR PLATFORM TESTING 19
FIGURE 24 3D VIEW OF THE SPAR SIMULATION MODEL 20
FIGURE 25 WAVE HEIGHT (M) VS DISTANCE FROM GATE (M) (SIMULATION VS EXPERIMENT) AT TIME = 2.5 SEC 23
FIGURE 26 WAVE HEIGHT (M) VS DISTANCE FROM GATE (M) (SIMULATION VS EXPERIMENT) AT TIME = 3.0 SEC 23

FIGURE 27 WAVE HEIGHT (M) VS DISTANCE FROM GATE (M) (SIMULATION VS EXPERIMENT) AT TIME = 3.26 SEC 23
FIGURE 28 WAVE HEIGHT (M) VS DISTANCE FROM GATE (M) (SIMULATION VS EXPERIMENT) AT TIME = 3.54 SEC 23
FIGURE 29 WAVE HEIGHT (M) VS DISTANCE FROM GATE (M) (SIMULATION VS EXPERIMENT) AT TIME = 3.66 SEC 24
FIGURE 30 WAVE HEIGHT (M) VS DISTANCE FROM GATE (M) (SIMULATION VS EXPERIMENT) AT TIME = 3.80 SEC 24
FIGURE 31 WAVE HEIGHT (M) VS DISTANCE FROM GATE (M) (SIMULATION VS EXPERIMENT) AT TIME = 5.00 SEC 24
FIGURE 32 2D VIEW OF DAM BREAK FLOW AT TIME = 0.0 SEC 25
FIGURE 33 PROTOCOL OF DUALSPHYSICS SIMULATIONS 26
FIGURE 34 VISUALIZATION OF DAM BREAK USING PARAVIEW AT TIME = 0.1 SEC 27
FIGURE 35 VISUALIZATION OF DAM BREAK USING PARAVIEW AT TIME = 0.2 SEC 27
FIGURE 36 COMPARISON BETWEEN SIMULATION AND EXPERIMENTAL DAM BREAK AT TIME = 0.1 SEC 27
FIGURE 37 COMPARISON BETWEEN SIMULATION AND EXPERIMENTAL DAM BREAK AT TIME = 0.2 SEC 27
FIGURE 38 VISUALIZATION OF DAM BREAK USING PARAVIEW AT TIME = 0.3 SEC 28
FIGURE 39 VISUALIZATION OF DAM BREAK USING PARAVIEW AT TIME = 0.4 SEC 28
FIGURE 40 VISUALIZATION OF DAM BREAK USING PARAVIEW AT TIME = 0.5 SEC 28
FIGURE 41 COMPARISON OF SIMULATION AND EXPERIMENTAL DAM BREAK AT TIME = 0.3 SEC 28
FIGURE 42 COMPARISON OF SIMULATION AND EXPERIMENTAL DAM BREAK AT TIME = 0.4 SEC 28
FIGURE 43 COMPARISON OF SIMULATION AND EXPERIMENTAL DAM BREAK AT TIME = 0.5 SEC 28
FIGURE 44 VISUALIZATION OF DAM BREAK USING PARAVIEW AT TIME = 0.6 SEC 29
FIGURE 45 VISUALIZATION OF DAM BREAK USING PARAVIEW AT TIME = 0.7 SEC 29
FIGURE 46 VISUALIZATION OF DAM BREAK USING PARAVIEW AT TIME = 0.8 SEC 29
FIGURE 47 COMPARISON OF SIMULATION AND EXPERIMENTAL DAM BREAK AT TIME = 0.6 SEC 29
FIGURE 48 COMPARISON OF SIMULATION AND EXPERIMENTAL DAM BREAK AT TIME = 0.7 SEC 29

FIGURE 49 COMPARISON OF SIMULATION AND EXPERIMENTAL DAM BREAK AT TIME = 0.8 SEC 29
FIGURE 50 VISUALIZATION OF DAM BREAK USING PARAVIEW AT TIME = 0.9 SEC 30
FIGURE 51 VISUALIZATION OF DAM BREAK USING PARAVIEW AT TIME = 1.0 SEC 30
FIGURE 52 COMPARISON OF SIMULATION AND EXPERIMENTAL DAM BREAK AT TIME = 0.9 SEC 30
FIGURE 53 COMPARISON OF SIMULATION AND EXPERIMENTAL DAM BREAK AT TIME = 1.0 SEC 30
FIGURE 54 GENERATED MODEL FOR SPAR PLATFORM SIMULATION 32
FIGURE 55 3D VIEW OF GENERATED SPAR PLATFORM ON SLOPED SEABED 32
FIGURE 56 SPAR PLATFORM DIMENSIONS 34
FIGURE 57 REFERENCE LINE FOR INITIAL POSITIONS OF SPAR 35
FIGURE 58 SPAR PLATFORM AT 0.18 M WATER DEPTH AT TIME = 0.0 SEC 35
FIGURE 59 SPAR PLATFORM AT 0.14 M WATER DEPTH AT TIME = 0.0 SEC 35
FIGURE 60 SPAR PLATFORM AT 0.1 M WATER DEPTH AT TIME = 0.0 SEC 36
FIGURE 61 SPAR PITCH VS TIME AT WATER DEPTH 0.18 M (D3) 37
FIGURE 62 SPAR PITCH VS TIME AT WATER DEPTH 0.14 M (D2) 37
FIGURE 63 SPAR PITCH VS TIME AT WATER DEPTH 0.10 M (D1) 37
FIGURE 64 COMPARISON BETWEEN PITCH OF SPAR AT DIFFERENT WATER DEPTHS . 38
FIGURE 65 INITIAL POSITION OF THE SPAR 39
FIGURE 66 SPAR PITCH VS TIME AT WAVE FREQUENCY 1.0 WAVES/SEC 40
FIGURE 67 SPAR PITCH VS TIME AT WAVE FREQUENCY 1.5 WAVES/SEC 40
FIGURE 68 SPAR PITCH VS TIME AT WAVE FREQUENCY 2.0 WAVES/SEC 40
FIGURE 69 COMPARISON BETWEEN PITCH OF SPAR AT DIFFERENT WAVE FREQUENCIES 41
FIGURE 70 INITIAL POSITION OF SPAR AT ALL WAVE AMPLITUDES 42
FIGURE 71 SPAR PITCH VS TIME AT WAVE AMPLITUDE V = 20 DEGREES 43
FIGURE 72 SPAR PITCH VS TIME AT WAVE AMPLITUDE V = 30 DEGREES 43
FIGURE 73 SPAR PITCH VS TIME AT WAVE AMPLITUDE V = 40 DEGREES 43
FIGURE 74 COMPARISON BETWEEN PITCH OF SPAR AT DIFFERENT WAVE AMPLITUDES 44

Chapter 1

Introduction

1.1 Background of Study

Production of oil and gas in the oceans requires offshore platforms or structures. Offshore structures come in various form factors ranging from fixed jacket platforms to floating semi-submersibles and Floating Storage and Offloading vessels (FPSO). Offshore structures are generally defined as structures that are installed in the oceans to exploit oil and gas reserves extracted from the subsea surface. As illustrated in Figure 1, there are several types of offshore structures utilized today depending on wave conditions, water depth and future field development.

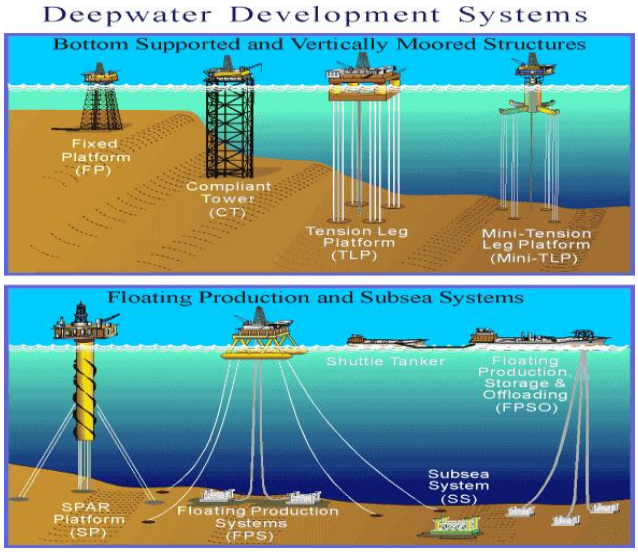

Figure 1 Types of Offshore Structures

Each and every offshore structure is unique in terms of its dimensions and oceanic conditions that it is designed for. Therefore, it is vital for the wave impact pressures to be simulated when designing and installing offshore structures (De Chowdhury & Sannasiraj, 2013). Simulating offshore models in controlled environments can reduce costs of real-time operational failure costs and prevent catastrophic asset losses in the field. Simulation of nonlinear wave patterns can be carried out by two methods; Smoothed Particle Hydrodynamics (SPH) by Gingold and Monaghan (1977) and Moving Particle Semi-Implicit Method (MPS) by Koshizuka and Oka (1996).

Simulations using the Smoothed Particle Hydrodynamics method (SPH) can help designers understand the potential risks and forces acting on the offshore structure during installation and throughout its service life.

1.2 Problem Statement

Offshore floating structures such as semi-submersibles, gravity base structures and spars are constantly subjected to forces due to wave loadings. Extreme wave loading on buoys has been simulated using the SPH method by previous researchers (Campbell, Vignjevic, & Patel, 2008). Extreme wave loading can lead to platform instability due to extreme wave heights and green-water accumulation on topside deck. However, there is an absence of research on the effect of extreme wave loading on the angular pitch of complex offshore floating structures such as SPARs in South East Asia (Campbell et al., 2008).

1.3 Objectives and Scope of Study

1.3.1 Objectives

- To validate the Smoothed Particle Hydrodynamics Method for project use.
- To construct a simulation model that replicates the wave reactions of deep-water floating SPAR Platforms
- To identify a relationship between varying wave amplitude, water depth and wave frequency to the angular pitch of deep-water SPARs.

1.3.2 Scope of study

In this paper, a numerical investigation of the structural responses of offshore floating structures subject to extreme wave loadings is presented. The results shall be validated against the data from experiments conducted by Pablo A. Caron (2015) and Ozmen-Cagatay and Kocaman (2011). Only highly non-linear waves following wave conditions in Asia-Pacific shall be studied in the paper.

Chapter 2

Literature Review

2.1 Offshore floating structures

In the oil and gas industry, offshore floating structures are defined as floating structures that maintain their position on the sea surface through the means of buoyancy and as such are used for the exploration, drilling, production, processing and storage of oil and gas production fluids. Offshore floating structures are common in water depths of more than 1700 ft or 520 m as fixed platforms are non-feasible in terms of cost (Karsan, Valdivieso, & Suhendra, 1986).

2.2 Types of offshore floating structures

2.2.1 Floating Production, Storage and Offloading Vessels (FPSO)

Floating production, storage and offloading vessels also known as FPSOs are shipping tankers converted into oil and gas production facilities which may include onboard processing of the production fluids, which are subsequently stored onboard for offloading onshore (Mastrangelo & Henriques, 2000). FPSOs are an extremely popular choice for developing marginal, fast-track, deep-water fields in areas of the ocean where it would not be feasible to construct pipelines (Knowles, Selwa, & Bankes, 1999).

2.2.2 Semi-submersibles

Semi-submersibles are offshore floating platforms generally with a submerged pontoon which provides buoyancy to the platform while thrusters subsea provide thrust to maintain the structure in its position from six degrees of freedom. As illustrated in Figure 2, the semi-submersible is similar to a ship in terms of how it maintains its trajectory and location.

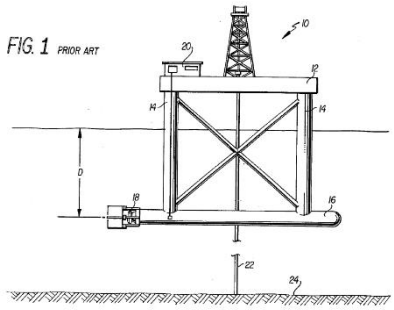

Figure 2 Semi Submersible Platform
(Haselton, 1976)

2.2.3 SPAR Platforms

Spar platforms are cylindrical floating structures moored to the seabed using vertical or catenary lines. Spar platforms are extremely versatile in deep-water production applications, especially in the Gulf of Mexico (Islam, Jameel, Jumaat, Shirazi, & Salman, 2012). One of the Spars used in the South East Asia region is the Kikeh Spar in Malaysia. Spars are categorized into 2 basic types; Classic Spar and Truss Spar. As illustrated in Figure 3, Spars generally have a cylindrical build.

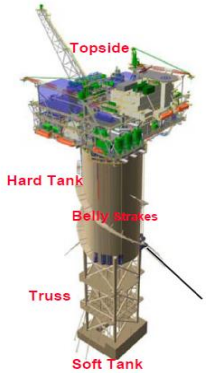

Figure 3 Typical Spar Platform Build
(Narold, Willemse, & Brenninkmeijer)

2.3 Wave loading on offshore floating structures

Extreme wave loading and green water loading are the major causes of damage to offshore floating structures used in the oil and gas industry (Buchner & Bunnik, 2007; Campbell et al., 2008; Cao & Wan, 2012; Guilcher, Couty, Brosset, & Le Touzé, 2012; Jian, Liang, & Shao, 2011; Thilleul et al., 2015). Extreme waves are extremely hard to predict and are a serious threat to offshore activities such as drilling and oil production (Cao & Wan, 2012).Conventionally, extreme wave and green water loading simulations are done using real-time models equipped with wave probes and accelerometers in wave tanks, however software analyses can help to reduce the number of models required for wave tank testing by helping researchers understand the general structural response to extreme waves (Rudman & Cleary, 2009).

2.4 Software-aided simulation methods

Computer aided engineering is a fundamental part of modern engineering. Computer simulations are able to calculate vast number of scenarios in a short number of time, saving precious resources used in futile real-time simulations. Computer simulations help researchers narrow down on the appropriate test models for real-time testing, saving cost and manpower (Rudman & Cleary, 2009). There are several types of simulation methods used however only Smoothed Particle Hydrodynamics (SPH) shall be used in this study as it presents researchers with a mesh less solution to complex fluid problems with dynamic boundaries (Campbell et al., 2008; Ma, Yan, Zhou, Duan, & Zheng, 2009).

2.4.1 Smoothed Particle Hydrodynamics (SPH) Method

Smoothed Particle Hydrodynamics (SPH) is a numerical method used for the approximate integration of the governing partial differential equations of continuum mechanics (Campbell et al., 2008; Gingold & Monaghan, 1977). It was originally developed by Gingold and Monaghan (1977) for the use in astrophysics. Since then it has been adapted for various uses, mainly for providing a Lagrangian method for calculating derivatives without a computational mesh. The SPH method has been used in studies of wave impact pressures, structural responses to wave loadings and sloshing of fluids in LNG tanks. The use of SPH schemes has been popular in the research of free surface flows with very large and rapid deformations.

2.4.2 Governing Equations

The Smoothed Particle Hydrodynamics (SPH) method is based on a technique called integral interpolation (Jian et al., 2011).The fluid domain is comprised of a finite number of separate particles.

$$f(x) = \int_{\Omega} f(x')\delta(x - x')dx'$$

With the kernel function included:

$$f(x) = \int_{\Omega} f(x')W(x - x', h)dx'$$

Where f is a function of the position vector and Ω is the integral volume that contains x.

2.4.3 Weakly Compressible SPH algorithm

The governing equations for a viscous fluid model are given as below:

$$\frac{D\rho}{Dt} = -\rho\nabla\cdot\bar{u}$$
$$\frac{D\bar{u}}{Dt} = -\frac{1}{\rho}\nabla\bar{p} + \nabla\cdot(\upsilon\nabla\bar{u}) + F^e$$

Equation 1 Navier Stokes Equations in WCSPH

Where ū is the Reynolds averaged velocity field, $\bar{p}$ is Reynolds averaged pressure field, υ is the kinematic viscosity and F^e is the external body force.

Equation of state to approximate fluid in the weakly compressible SPH:

$$p = B\left(\left(\frac{\rho}{\rho_0}\right)^{\gamma} - 1\right)$$

Equation 2 Equation of State in WCSPH

Where p_0 is the nominal water density of 1000 kg/m^3 while B is defined as $p_o C_s^2/\gamma$. γ is the adiabatic factor assumed as 7. C_s is the assumed numerical speed of sound in the medium.

2.4.4 Kernel Function Approximation in SPH

In order to change the Partial Differential Equations of the problem to an equivalent particle interaction model in the form of Ordinary Differential Equations, a distribution function is interpolation from the surrounding set of neighboring points. This function is known as the kernel function. In this paper, the renormalized Gaussian is used.

2.4.5 Artificial Viscosity

In Smoothed Particle Hydrodynamics, artificial viscosity is introduced by Gingold and Monaghan (1977).

$$\begin{cases} \Pi_{ij} = \begin{cases} \dfrac{-\alpha' \overline{c}_{ij} \zeta_{ij} + \beta \zeta_{ij}^{\,2}}{\overline{\rho}_{ij}}, & \boldsymbol{v}_{ij}.\boldsymbol{r}_{ij} \le 0 \\ 0, & \boldsymbol{v}_{ij}.\boldsymbol{r}_{ij} > 0 \end{cases} \\ \zeta_{ij} = \dfrac{h\boldsymbol{v}_{ij}.\boldsymbol{r}_{ij}}{\left|\boldsymbol{r}_{ij}\right|^2 + \kappa^2}, \overline{c}_{ij} = (c_i + c_j)/2, \overline{\rho}_{ij} = (\rho_i + \rho_j)/2 \end{cases}$$

Equation 3 Artificial Viscosity

Artificial viscosity may degrade the results in non-violent cases but has little effect on the results in violent cases such as extreme waves.

2.5 Effect of Relative Wave Height and Air Gap to the Wave Impact Pressure

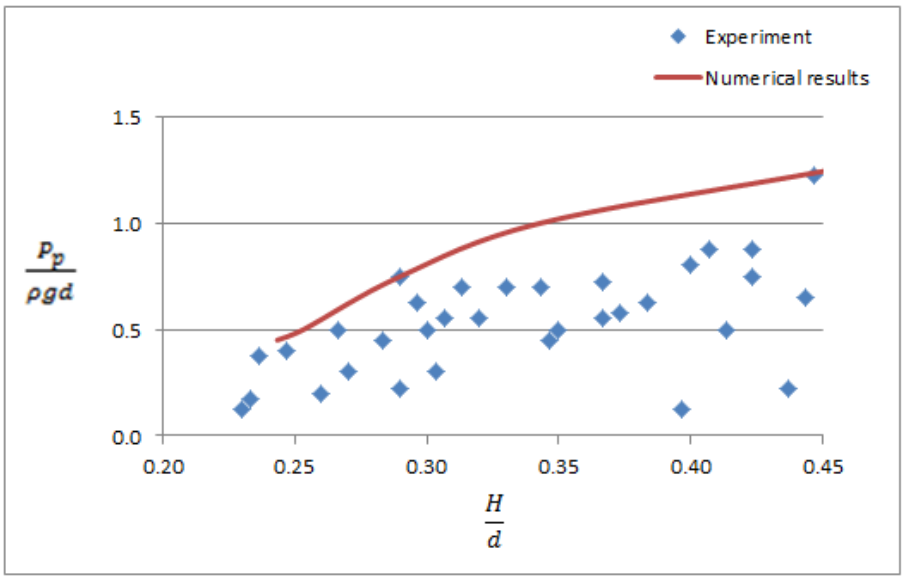

Figure 4 Comparison of Normalized peak pressure with experiments

Referring to Figure 4, scattered points are experimental data and the solid curve is numerical results. There is a scattering of data from experimental results showing the complexity of obtaining a consistent result for all cases. The computational results envelop the experiment data may be caused by the energy losses due to turbulence as they are not considered in the numerical model.

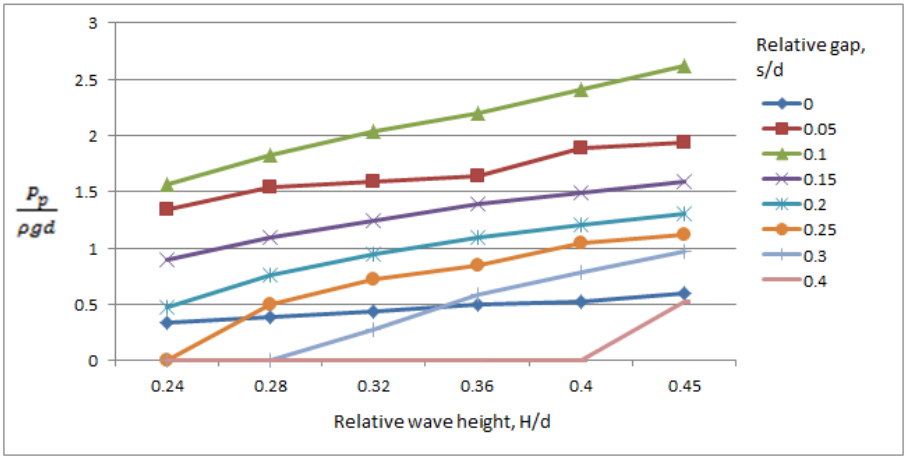

Figure 5 Impact Peak Pressure P_p/ρgd with H/d and s/d (Wang, 1996)

The impact peak pressure $P_p/\rho gd$ with H/d and s/d is as shown in Figure 5. The impact pressure increases with increasing relative wave height.

2.5.1 Effect of Wave Height on the Wave Impact Load to the Platforms

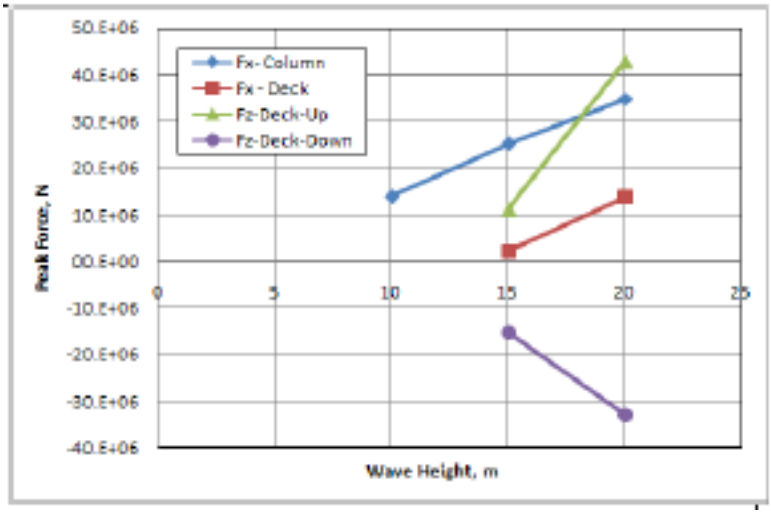

Figure 6 Peak force versus wave height
[Fx = horizontal load, Fz = vertical load] (Lubeena & Gupta, 2013)

Figure 6 shows the peak force on the column and deck of the platform structure for different wave height. It also shows the total horizontal and vertical forces exerted on the platform. The wave impact force exerted greater vertical load to the platform than the horizontal load.

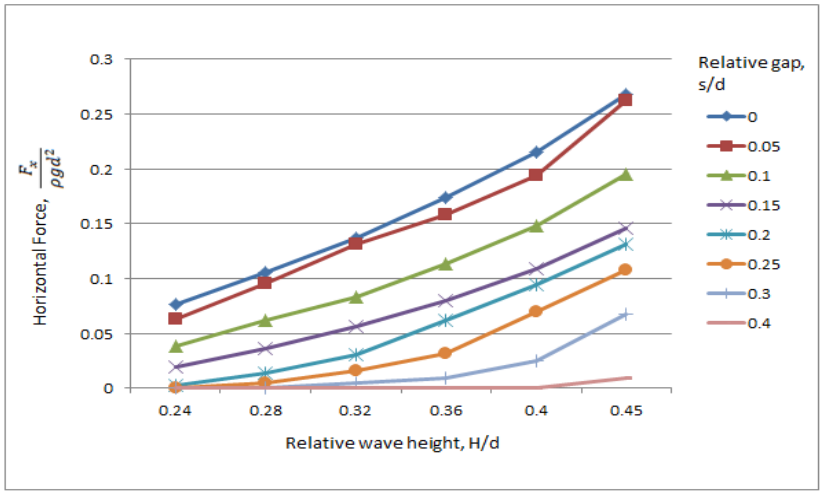

Figure 7 Horizontal Force $\frac{F_x}{\rho g d^2}$ with H/d and s/d (Wang, 1996)

Wang (1996) ran simulations to simulate the horizontal force and vertical force on the platform by varying the relative wave height and relative gap. The results as shown in Figure 7 and Figure 8 show that the forces on the platform increase with increasing relative wave height.

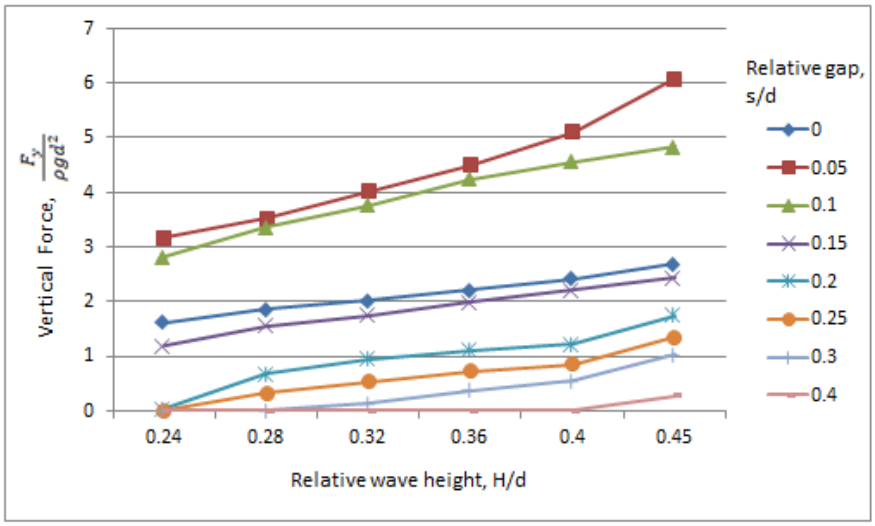

Figure 8 Vertical Force $\frac{F_y}{\rho g d^2}$ with H/d and s/d (Wang, 1996)

Chapter 3

Methodology

3.1 FYP Gantt Chart & Project Key Milestones

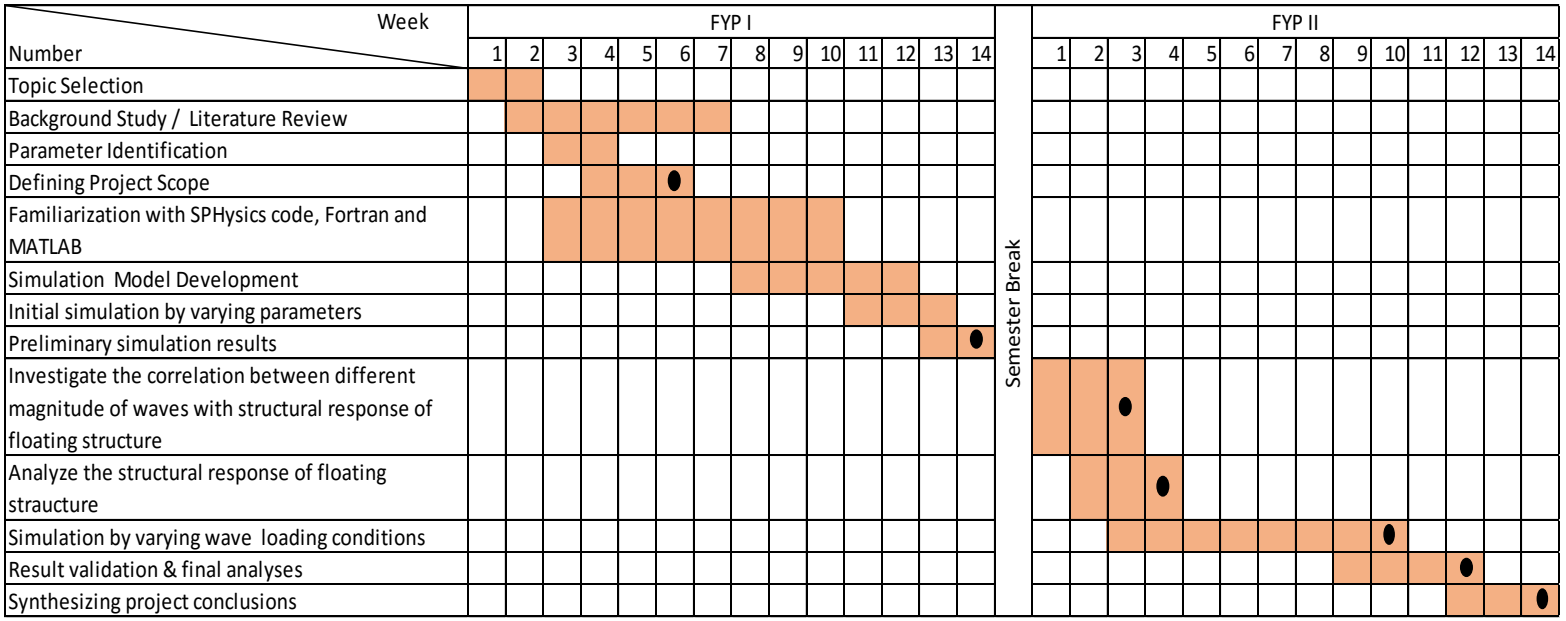

* ● denotes key milestones

3.2 FYP Flowchart

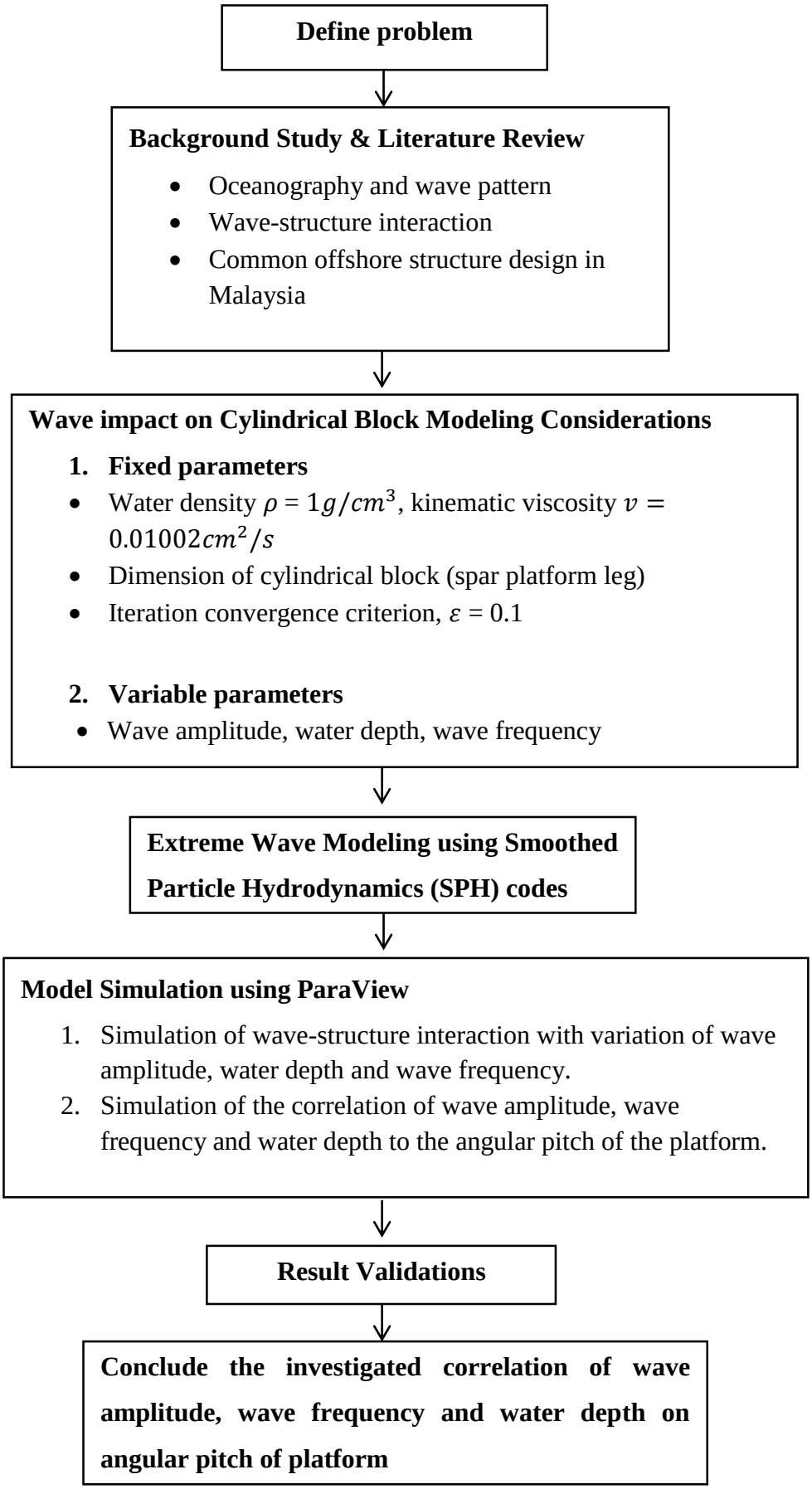

3.3 Validation Example 1 : Dam Break with Trapezoid Obstacle

In order to prove that the designed SPH model is able to simulate real-time conditions to a considerable accuracy, validation of the SPH model is required. This is done by comparing the data obtained from real-time experimental data and simulation data from SPH model calculations.

A model simulating a dam break condition is simulated using the SPH model while a real-time wave tank with a dam-break mechanism set-up was utilized.

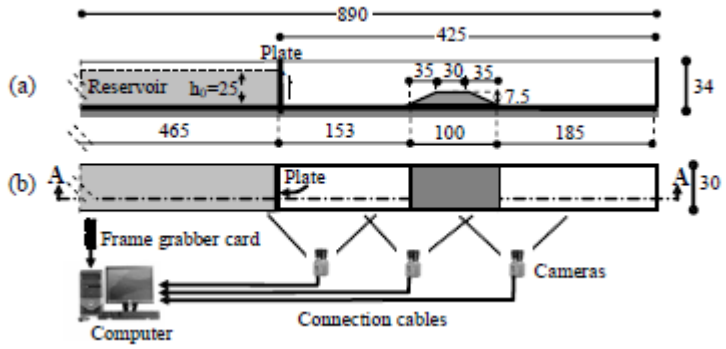

Figure 9 The Experimental Set-up of Dam Break Mechanism (Ozmen-Cagatay & Kocaman, 2011)

3.3.1 Initial and Boundary Conditions

The dimensions of the experimental set-up area as shown in Figure 9. As for the simulation set-up, the dimensions of the fluid domain for the SWE model is 8.9m long and 0.5m high. The fluid column to be initially 4.65m long by 0.25m high. A trapezoidal shape of 0.075 m high and 1 m base length is located 1.53 m downstream from the plate. The lower boundary was defined as a wall and the upper boundary as symmetry to allow atmospheric effects on the free surface. The channel sidewalls were assumed symmetry to imply no flux and shears. All surfaces are assumed smooth (Ozmen-Cagatay & Kocaman, 2011).

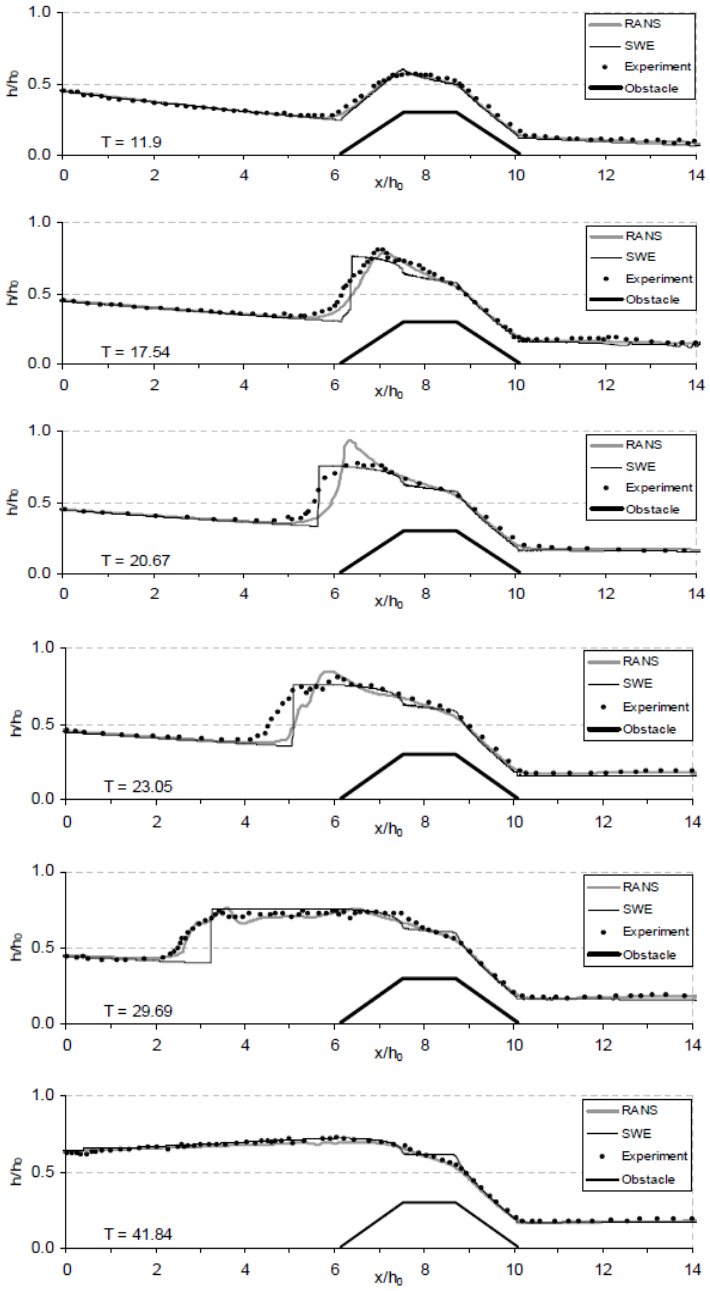

Figure 10 The computed surface profiles at different points of time (Ozmen-Cagatay & Kocaman, 2011)

As illustrated in Figure 10, the experimental data obtained is then compared with the simulation data for validation. This approach can be utilized to validate other SPH models by modifying the experimental set-up and SPH model conditions and input parameters.

3.4 Validation Example 2 : Dam Break Flow

The second validation example is a simple dam break flow problem. The simulation model is constructed in accordance with a real life experimental set-up carried out by Pablo A. Caron (2015).

The following figure shows the experimental set-up:

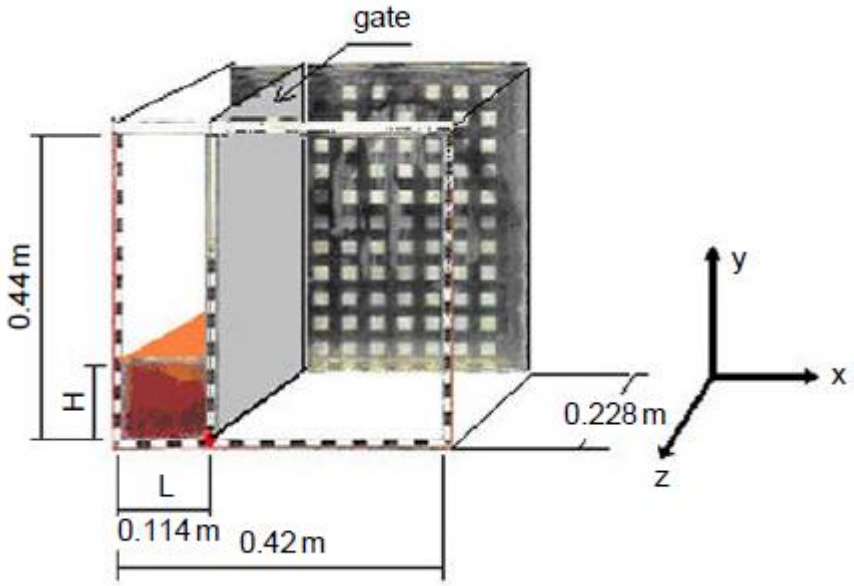

Figure 11 Experimental Set-up (Pablo A. Caron, 2015)

The water in the reservoir behind the gate is released when the gate is lifted up rapidly. A high speed camera is then used to take high speed photographs of individual timeframes of the water flow.

The individual timeframes are shown in the figures below:

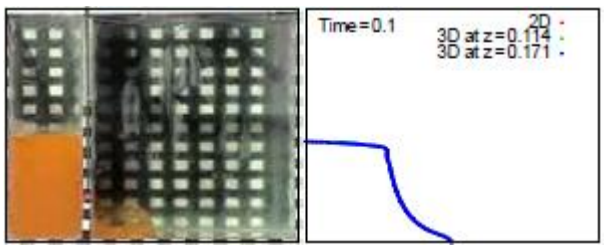

Figure 12 Dam Break at t=0.1 sec

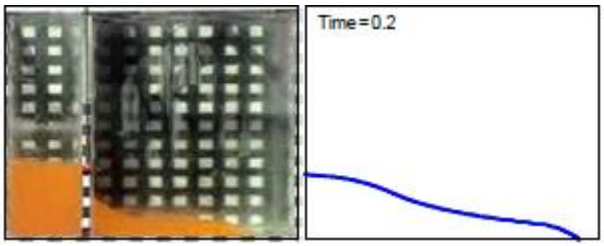

Figure 13 Dam Break at t=0.2 sec

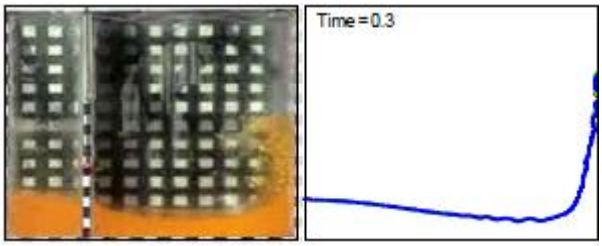

Figure 14 Dam Break at t=0.3 sec

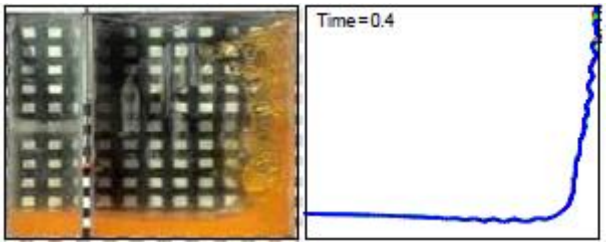

Figure 15 Dam Break at t=0.4 sec

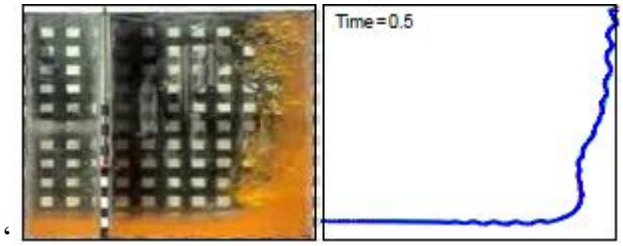

Figure 16 Dam Break at t=0.5 sec

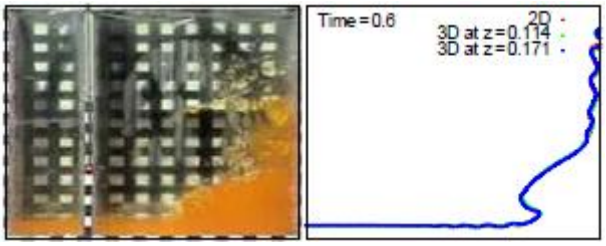

Figure 17 Dam Break at t=0.6 sec

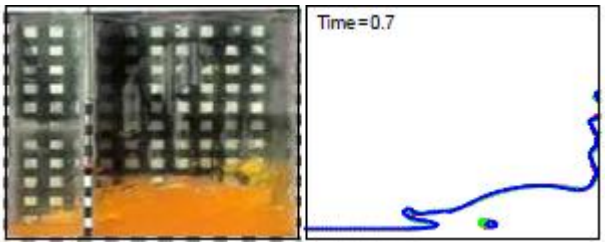

Figure 18 Dam Break at t=0.7 sec

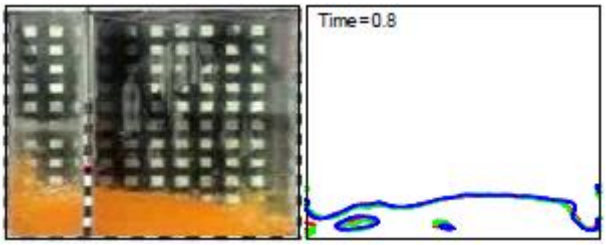

Figure 19 Dam Break at t=0.8 sec

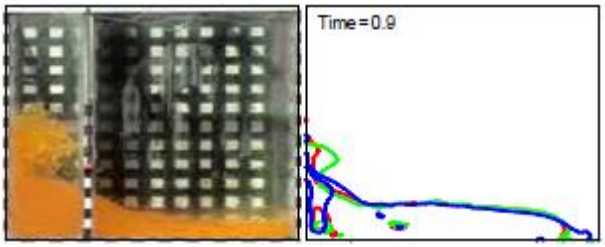

Figure 20 Dam Break at t=0.9 sec

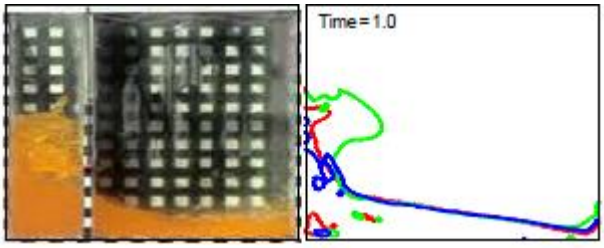

Figure 21 Dam Break at t=1.0 sec

The simulation model is then constructed with the exact dimensions and parameters as the experimental set-up and is run to match the timeframes selected in the paper by Pablo A. Caron (2015).

3.5 Development of Simulation Model

3.5.1 Model 1 (Sloped Shoreline)

The development of the 2D simulation model shall be based on Figure 22. The simulation shall be done with particle generation using the Smoothed Particle Hydrodynamics (SPH) model where the programming is done in the FORTRAN and Visual C++ language. This simulation utilizes the DualSPHysics platform. The following variables shall be changed during the simulation process:

- **Wave Amplitude of Piston-Flap. V**
- **Water Depth, d**
- **Wave Frequency, f**

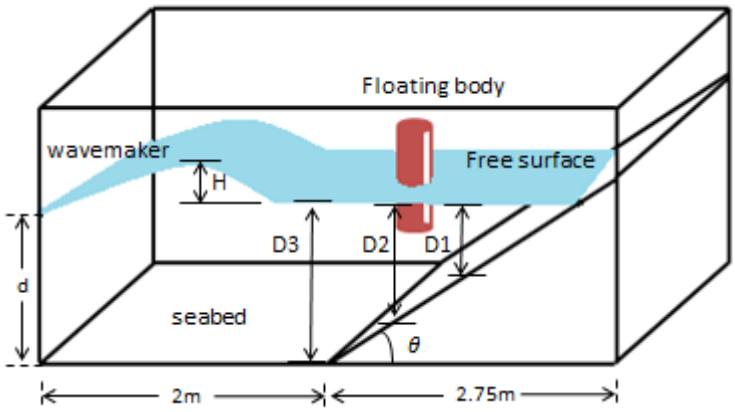

Figure 22 Proposed Model for SPAR Platform Simulation

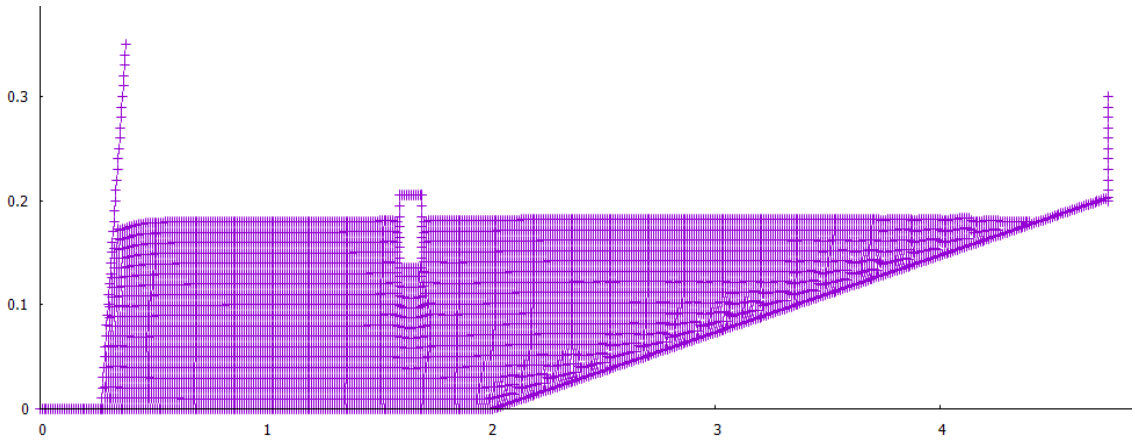

Figure 23 Generated Solution Domain for SPAR Platform Testing

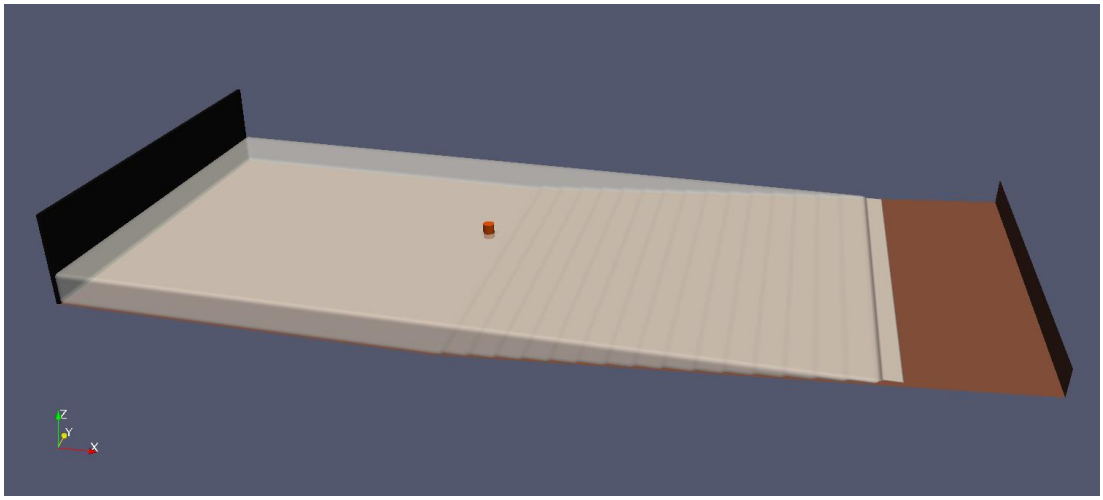

Figure 24 3D View of the SPAR Simulation Model

The main difficulties experienced during the development of this model are:

- The spacing used can affect the accuracy of the model. Spacing that are too small could also result in simulation times that are too long due to the high number of particles generated.
- The boundary conditions defined for the floating cylinder are dissimilar from conventional shapes such as boxes and cuboids. In order to obtain a good representation of the cylinder that does not leak, the lattice structure of the cylinder needs to be defined differently.

Chapter 4

Results & Discussion

4.1 Validation Results

4.1.1 Validation Example 1 (Dam Break with Trapezoid Obstacle)

The Smoothed Particle Hydrodynamics model was used to simulate the validation example experiment carried out. The following conditions were utilized:

This simulation for the validation example utilizes a Wendland kernel function without any kernel corrections. Each and every time step follows the Predictor-corrector algorithm with a max time runtime of 5.1 seconds and readings taken at every 0.02 second interval.

The simulation utilizes an artificial viscosity function with the main characteristics of the model derived from the Tait's Equation of State. The boundary conditions defined in this model are based on the Dalrymple forces without any filters used.

The geometry of the zone was defined as a box with the dimensions of 8.9 m x 0.7 m. The initial fluid structure was defined as a cube with dimensions of 4.65 m x 0.25 m with a spacing of 0.02 m for both x and y axes.

A trapezoidal obstacle was defined in the model with dimensions of 1.0 m base and 0.08 m in height. This was placed 1.53 m in front of the gate of height 0.34 m.

The model utilizes a double precision. The compiler used for this model is the Silverfrost FTN95.

The CaseN.txt file was utilized to input data into the SPHysicsgen_2D file to generate the objects required for the real-time simulation program of SPHysics_2D. The SPHysicsgen_2D program generated a number of files including:

- INDAT file
- IPART file
- Matlabin file
- Obstacle file
- Precision_kind.2D file
- SPHYSICS.mak file
- Tsunami_Landslide file
- Wavemaker file
- Gate file
- Floating_bodies file
- Normals.init

Using these files generated by the SPHysicsgen_2D program, the SPHysics_2D file is compiled using the information provided in the SPHYSICS.mak file to ensure that the object resources are compiled properly into the executable file.

The executable file (modelrun1.exe) was then run to generate PART_000N files for each and every time interval of 0.02 seconds according to the duration specified in the CaseN.txt file.

The PART_000N files are then used to generate plots using a software known as GnuPlot to visualize the motion of the fluid in the domain specified.

The simulation results for the validation example are as follows:

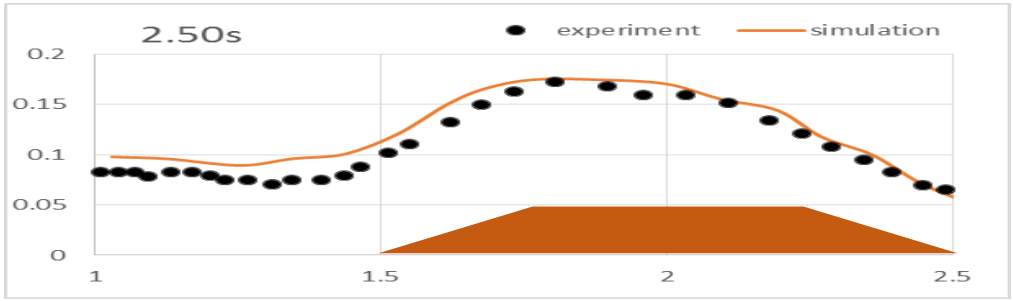

Figure 25 Wave height (m) vs Distance from gate (m) (Simulation vs Experiment) at Time = 2.5 sec

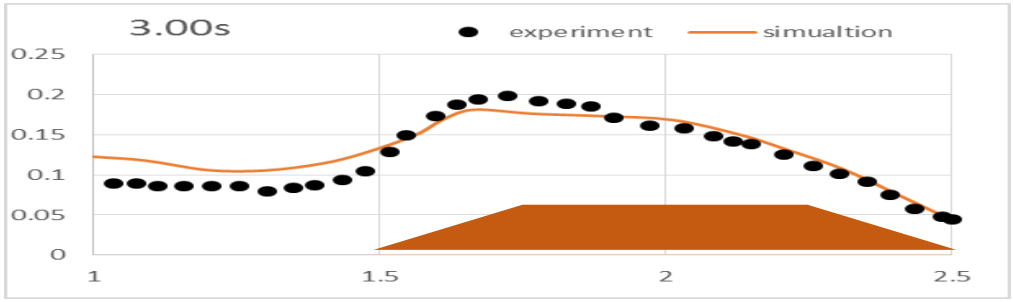

Figure 26 Wave height (m) vs Distance from gate (m) (Simulation vs Experiment) at Time = 3.0 sec

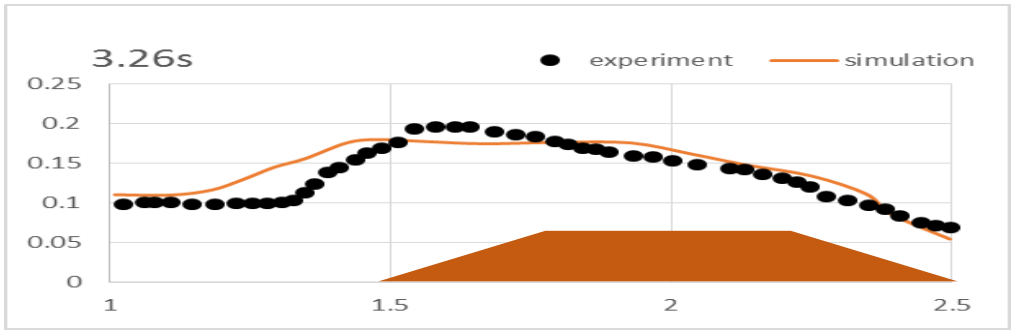

Figure 27 Wave height (m) vs Distance from gate (m) (Simulation vs Experiment) at Time = 3.26 sec

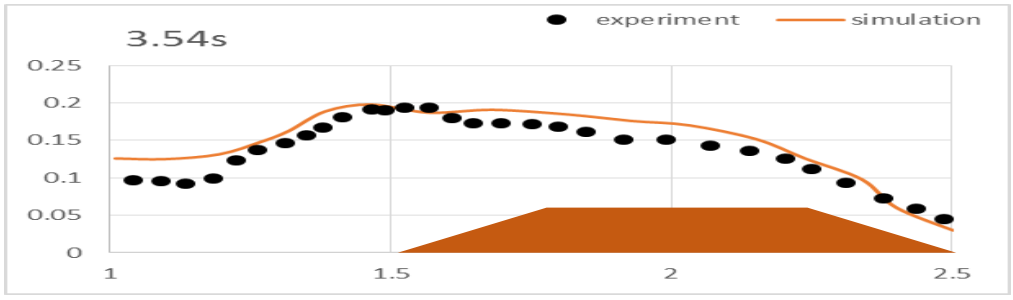

Figure 28 Wave height (m) vs Distance from gate (m) (Simulation vs Experiment) at Time = 3.54 sec

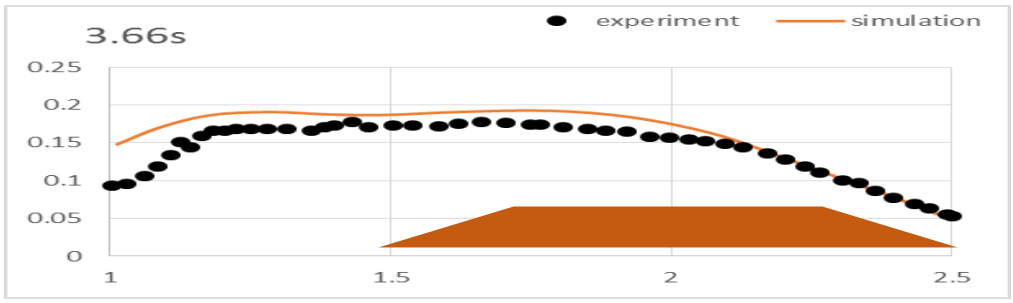

Figure 29 Wave height (m) vs Distance from gate (m) (Simulation vs Experiment) at Time = 3.66 sec

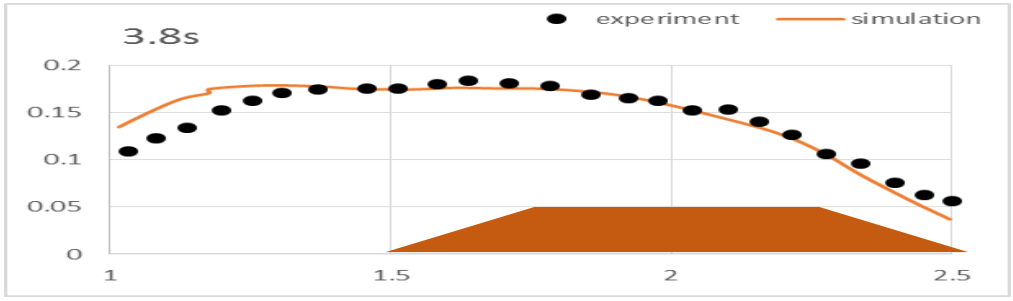

Figure 30 Wave height (m) vs Distance from gate (m) (Simulation vs Experiment) at Time = 3.80 sec

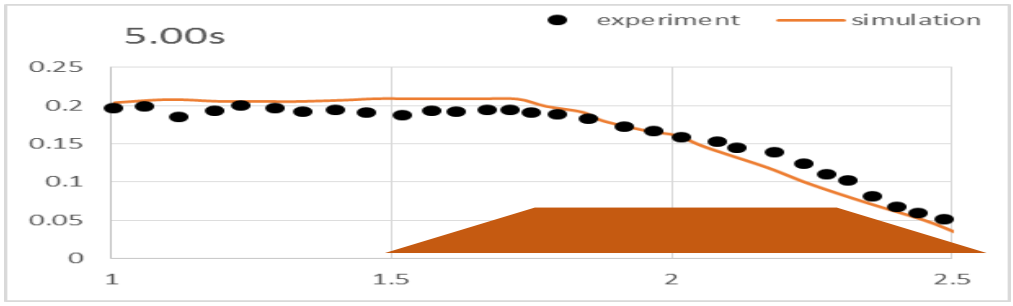

Figure 31 Wave height (m) vs Distance from gate (m) (Simulation vs Experiment) at Time = 5.00 sec

It can be observed from the plots generated through the validation example, the trapezoid induces a wave propagating backwards towards the source of the wave. This closely replicates the data from the validation example carried out by Ozmen-Cagatay and Kocaman (2011). The average percentage error for all the graphs is 6.954%. This is less than 10% and can be accepted.

4.1.2 Validation Example 2 (Dam Break Flow)

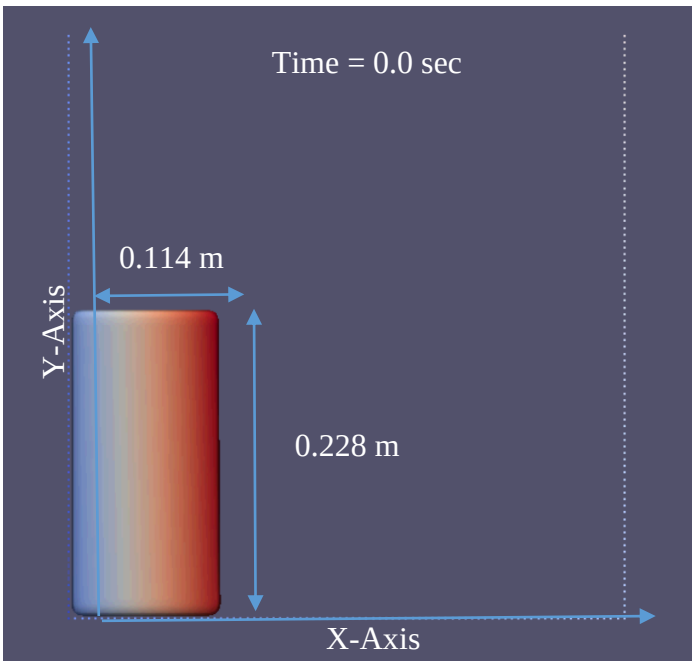

Figure 32 2D View of Dam Break Flow at time = 0.0 sec

The experimental set-up was modelled using the Smoothed Particle Hydrodynamics Method to determine whether the SPH method could replicate real-life experimental results.

This simulation for the validation example utilizes a Wendland kernel function without any kernel corrections. Each and every time step follows the Predictor-corrector algorithm with a max time runtime of 1.0 seconds and readings taken at every 0.02 second interval.

The simulation utilizes an artificial viscosity function with the main characteristics of the model derived from the Tait's Equation of State. The boundary conditions defined in this model are based on the Dalrymple forces without any filters used.

The geometry of the zone was defined as a box with the dimensions of 0.42 m x 0.44 m. The initial fluid structure was defined as a cube with dimensions of 0.114 m x 0.228 m with a spacing of 0.01 m for both x and y axes. The Aspect ratio of this set-up is 2.

The model utilizes a double precision. The compiler used for this model is the Microsoft Visual C++ compiler utilizing the Nvidia CUDA toolkit.

First, the Case_Floating_2D.xml file, which is lines of Visual C++ code is edited to change the case to fit our requirements for the simulated model. The GPU.bat file is then run to execute the instructions in the .exe files of the DualSPHysics package. The GenCase package then generates case files that are processed to generate part files. These part files are then packaged into vtk or Visualization Toolkit files for results visualization.

The figure below shows the flow of a typical DualSPHysics simulation.

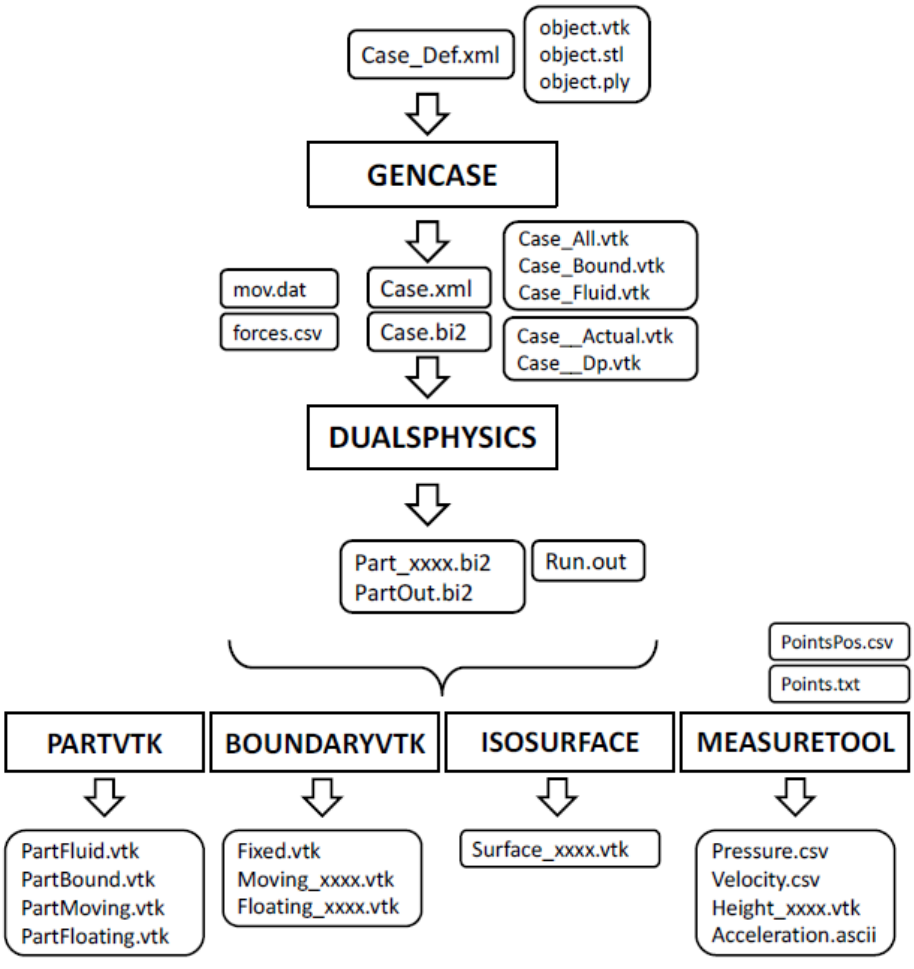

Figure 33 Protocol of DualSPHysics simulations

The .VTK files are then visualized using the ParaView program. The ParaView program is a powerful visualization and data analysis tool used by most researchers

around the world as it is able to visualize contours and vectors of massive amount of particles. This tool is especially useful for DualSPHysics visualizations as the number of particles are in the order of magnitude of 10^6.

The visualization of the results obtained from the simulation are shown in the figures that follow:

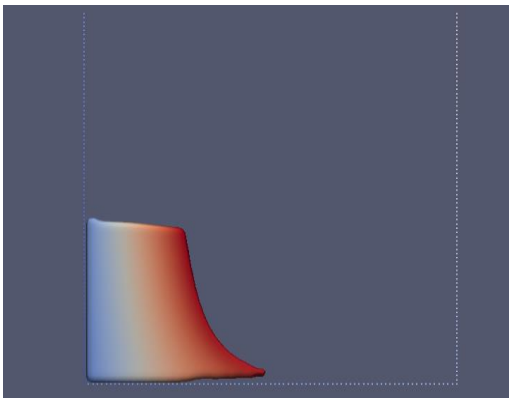

Figure 34 Visualization of Dam Break using ParaView at Time = 0.1 sec

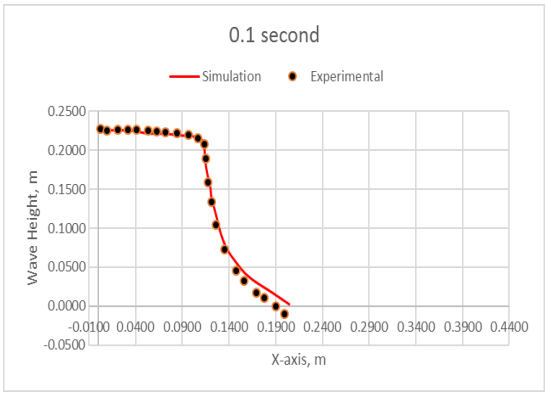

Figure 36 Comparison between Simulation and Experimental Dam Break at Time = 0.1 sec

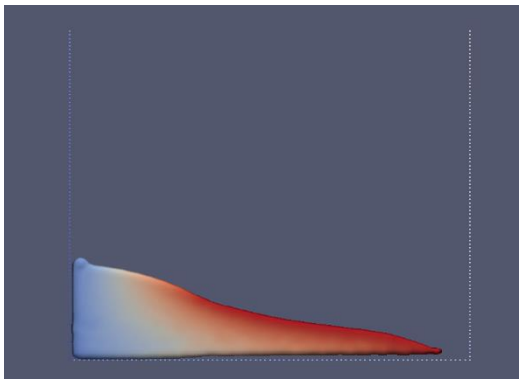

Figure 35 Visualization of Dam Break using ParaView at Time = 0.2 sec

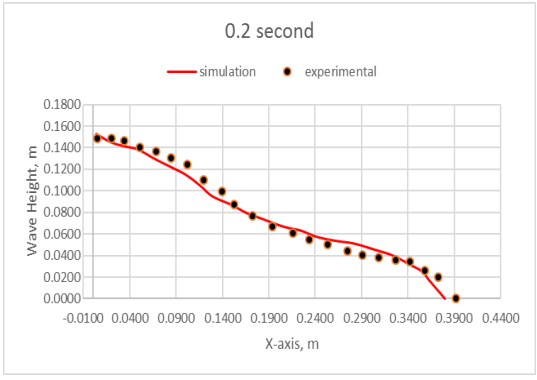

Figure 37 Comparison between Simulation and Experimental Dam Break at Time = 0.2 sec

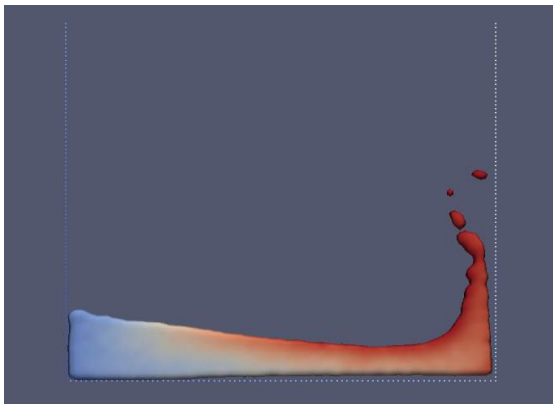

Figure 38 Visualization of Dam Break using ParaView at Time = 0.3 sec

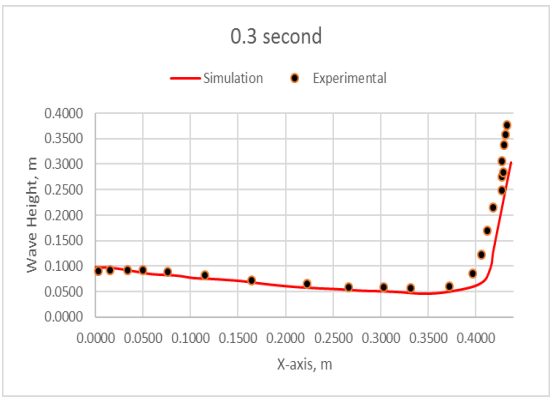

Figure 41 Comparison of Simulation and Experimental Dam Break at Time = 0.3 sec

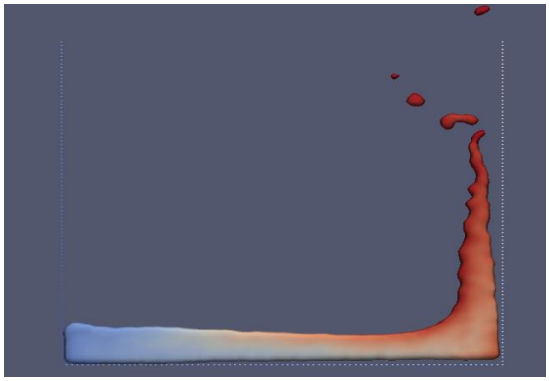

Figure 39 Visualization of Dam Break using ParaView at Time = 0.4 sec

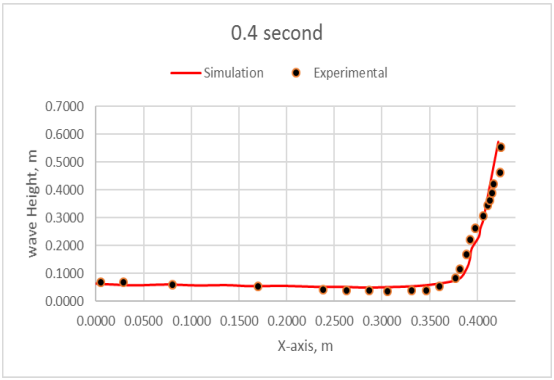

Figure 42 Comparison of Simulation and Experimental Dam Break at Time = 0.4 sec

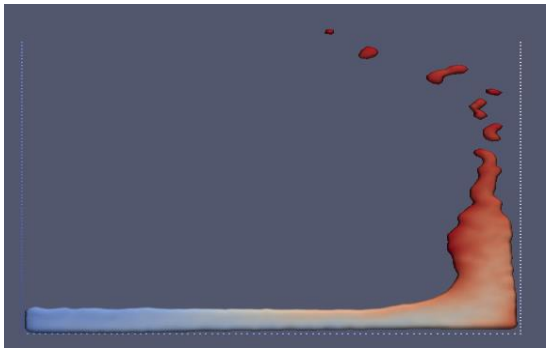

Figure 40 Visualization of Dam Break using ParaView at Time = 0.5 sec

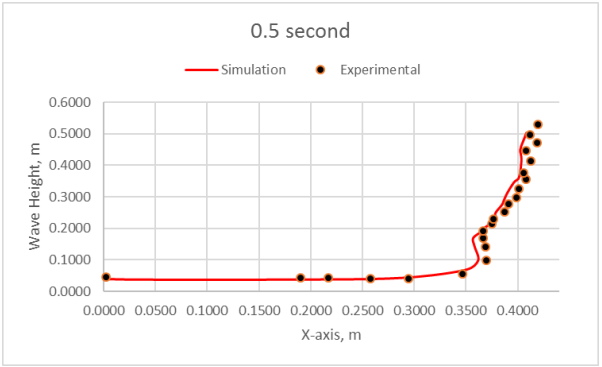

Figure 43 Comparison of Simulation and Experimental Dam Break at Time = 0.5 sec

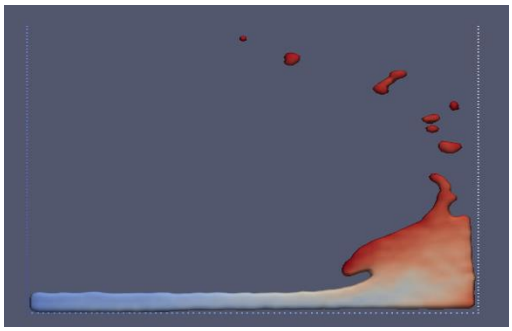

Figure 44 Visualization of Dam Break using ParaView at Time = 0.6 sec

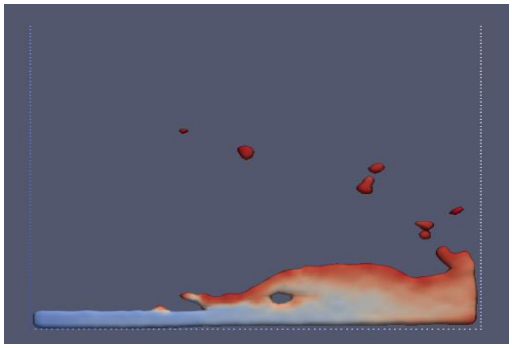

Figure 45 Visualization of Dam Break using ParaView at Time = 0.7 sec

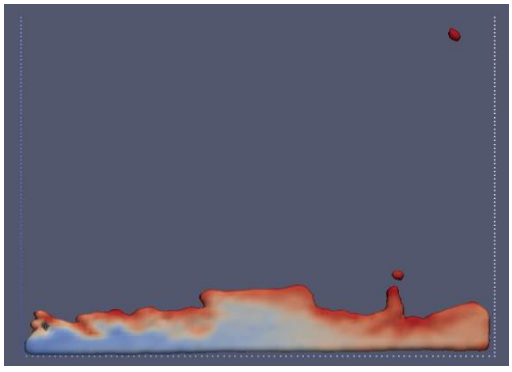

Figure 46 Visualization of Dam Break using ParaView at Time = 0.8 sec

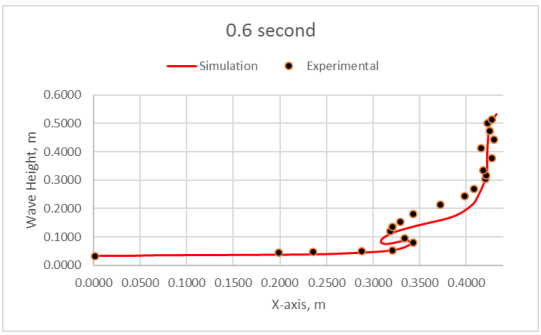

Figure 47 Comparison of Simulation and Experimental Dam Break at Time = 0.6 sec

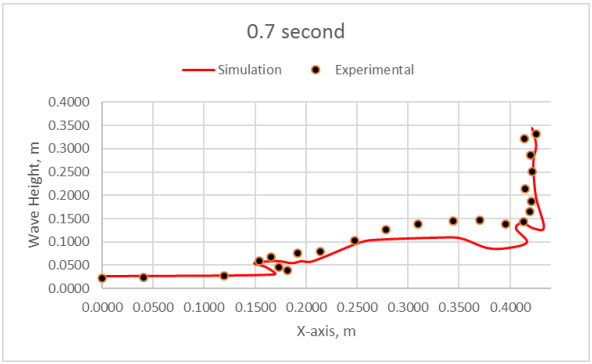

Figure 48 Comparison of Simulation and Experimental Dam Break at Time = 0.7 sec

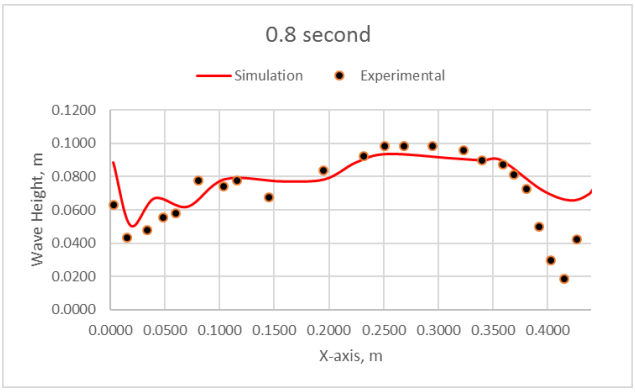

Figure 49 Comparison of Simulation and Experimental Dam Break at Time = 0.8 sec

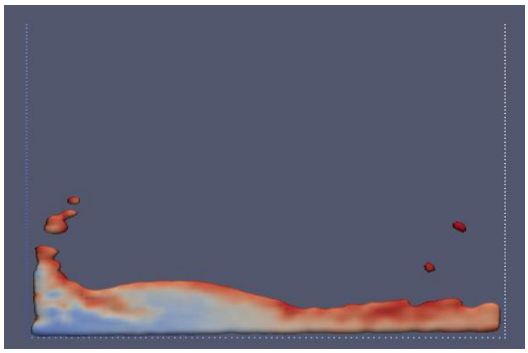

Figure 50 Visualization of Dam Break using ParaView at Time = 0.9 sec

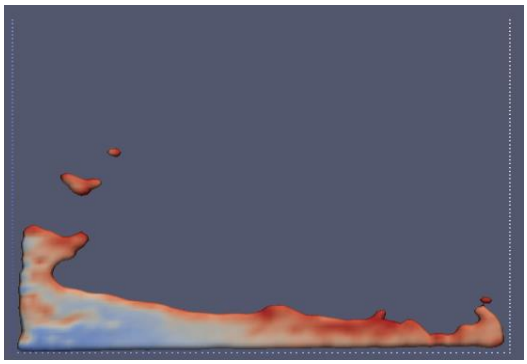

Figure 51 Visualization of Dam Break using ParaView at Time = 1.0 sec

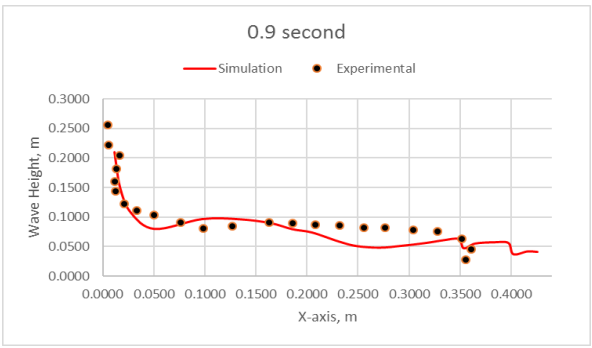

Figure 52 Comparison of Simulation and Experimental Dam Break at Time = 0.9 sec

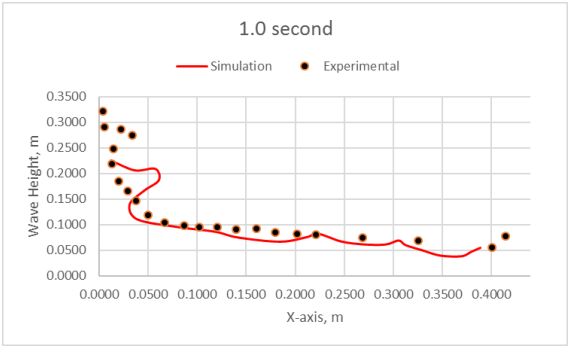

Figure 53 Comparison of Simulation and Experimental Dam Break at Time = 1.0 sec

The visualization of the simulation is converted into data points using a Matlab plugin known as Grabit.m. This Matlab plugin enables users to define values of axes on a photograph or image. After defining the range of the axes, the user is able to grab points from the image, showing values of the points grabbed. The experimental results are grabbed from the images taken by the high speed camera from research done by Pablo A. Caron (2015) as shown in **Figures 12 - 21**.

These points are then plotted into an Excel file in order to build the graphs that are seen on the right side of the pages 28 - 31.

As observed from the figures, the first five timeframes, t= 0.1 sec – 0.5 sec show fairly high similarities to the experimental data with very low errors in accuracy and consistency.

However, as the fluid propagates back from the gush up, the fluid starts to behave very violently from t= 0.6 sec – 1.0 sec. This violent nature of the fluid flow makes

extracting the data from the simulation extremely difficult and errors in this time region are significantly higher than the average error for the first five timeframes.

However, even with the violent behavior of the water from 0.6 sec – 1.0 sec, the average error for the entire simulation when compared to the experimental results has been calculated as 9.28%.

This error is considered to be relatively low considered that the errors are calculated by taking 10 points from the experiment and simulation and compared to each other to find the percentage error. The error is then averaged out by 10 timeframes representing 10 sets of data.

Therefore, it can be verified and concluded that the Smoothed Particle Hydrodynamics method can be used to closely simulate fluid flows and movements, even violent and turbulent ones given a high precision of parameters and high number of particles defined.

4.2 Simulation of SPAR Platform on a Beach or Sloped Seabed

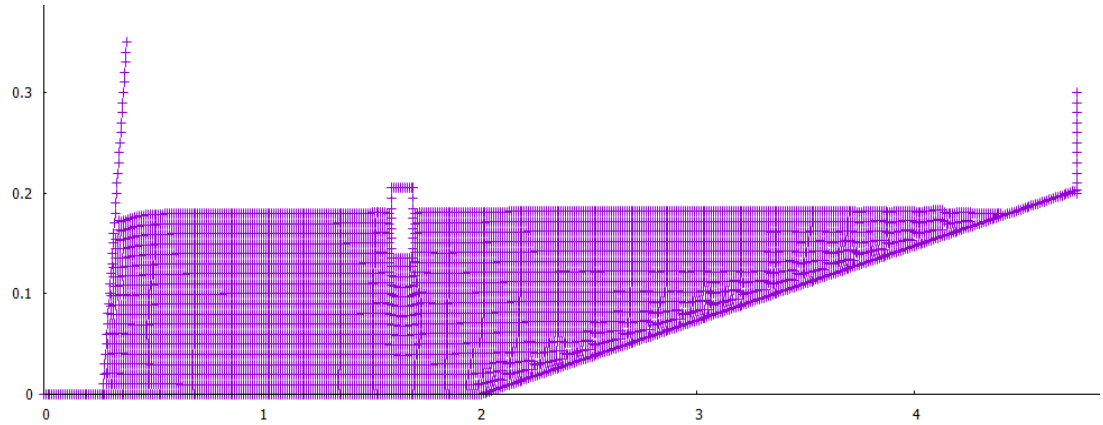

Figure 54 Generated Model for SPAR Platform simulation

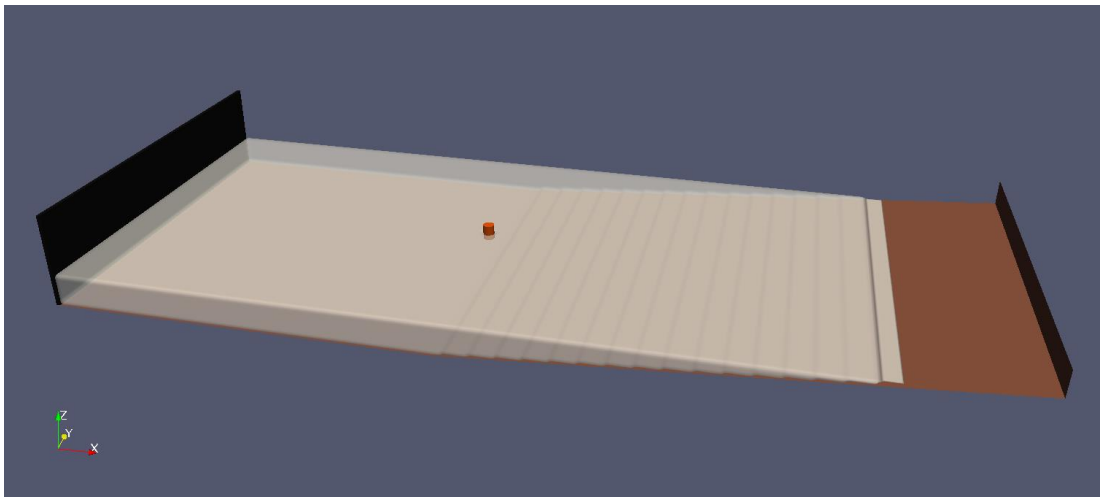

Figure 55 3D View of Generated Spar Platform on Sloped Seabed

This model was generated using the conditions as follows:

This simulation for the validation example utilizes a Wendland kernel function without any kernel corrections. Each and every time step follows the sympletic algorithm with a max time runtime of 3.5 seconds and readings taken at every 0.1 second interval.

The simulation utilizes an artificial viscosity function with the main characteristics of the model derived from the Tait's Equation of State. The boundary conditions defined in this model are based on the repulsive forces without any filters used.

The geometry of the zone was defined as a beach. The initial fluid structure was defined as a cube with dimensions of 4.75 m x 0.35 m with a spacing of 0.01 m for both x and y axes.

The beach was defined with an inclination of 4.2364 degrees. A wave maker was defined on the far left of the model with a piston.

A floating body is defined in the model as a square cylinder of dimensions 0.08 m (height) x 0.03 m (radius).

The model utilizes a double precision. The compiler used for this model is the Microsoft Visual C++ compiler utilizing the Nvidia CUDA toolkit.

First, the Case_Floating_2D.xml file, which is lines of Visual C++ code is edited to change the case to fit our requirements for the simulated model. The GPU.bat file is then run to execute the instructions in the .exe files of the DualSPHysics package. The GenCase package then generates case files that are processed to generate part files. These part files are then packaged into .vtk or Visualization Toolkit files for results visualization.

The .VTK files are then visualized using the ParaView program. The ParaView program is a powerful visualization and data analysis tool used by most researchers around the world as it is able to visualize contours and vectors of massive amount of particles. This tool is especially useful for DualSPHysics visualizations as the number of particles are in the order of magnitude of 10^6.

In this simulation, the fluid is converted from individual particles into a surface using the ISOSURFACE toolkit in the software for easier visualization and data analysis using Matlab Grabit.

This simulation was carried out by varying three main parameters; wave amplitude, wave frequency and water depth.

The values of the main parameters used are as shown in the table below:

Table 1 Parameters for Simulation

Input Parameters	Simulation
Model Scale ratio	1:6040
Water depth utilized (m)	0.10,0.14,0.18
Wave amplitude of piston-flap, V (°)	20, 30. 40
Equation of State	Tait's equation
ρ_{water} (kg/m^3)	1000
Boundary condition	Dalyrymple Repulsive force
Coefficient of friction, floating body	0.2
Floating body dimension LX, LZ (m)	0.06,0.08
Relative weight of SPAR ($^{\rho_{object}}/_{\rho_{water}}$)	1.0
Seabed slope angle, θ (°)	4.3
Coefficient of speed of sound	10
Frequency of wave (waves/sec)	1.0, 1.5, 2.0
Particle spacing (dx,dz)	0.02,0.02

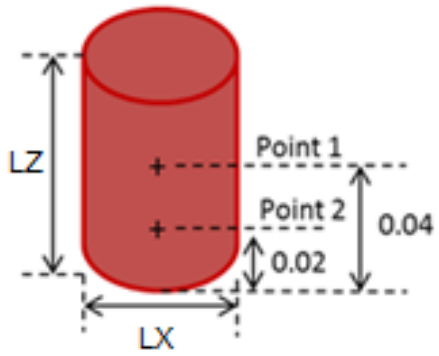

Figure 56 SPAR Platform Dimensions

4.3 Effect of Varying Water Depth on Angular Pitch of SPAR

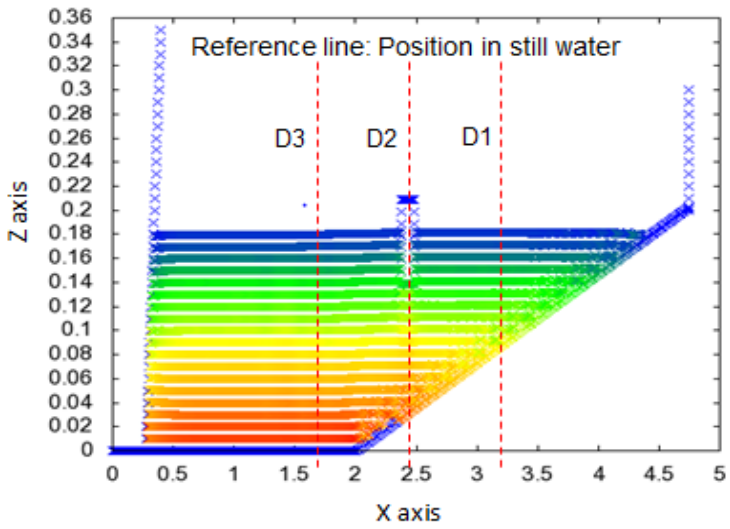

Figure 57 Reference Line for Initial Positions of SPAR

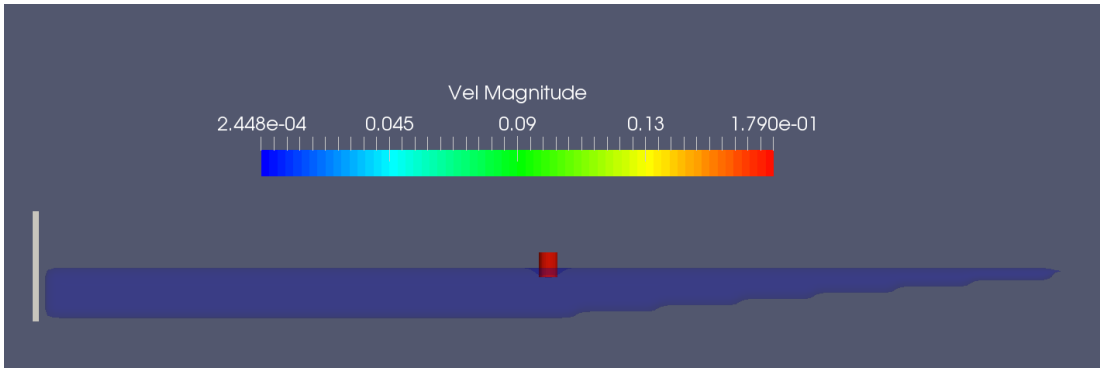

Figure 58 SPAR Platform at 0.18 M Water Depth at Time = 0.0 sec

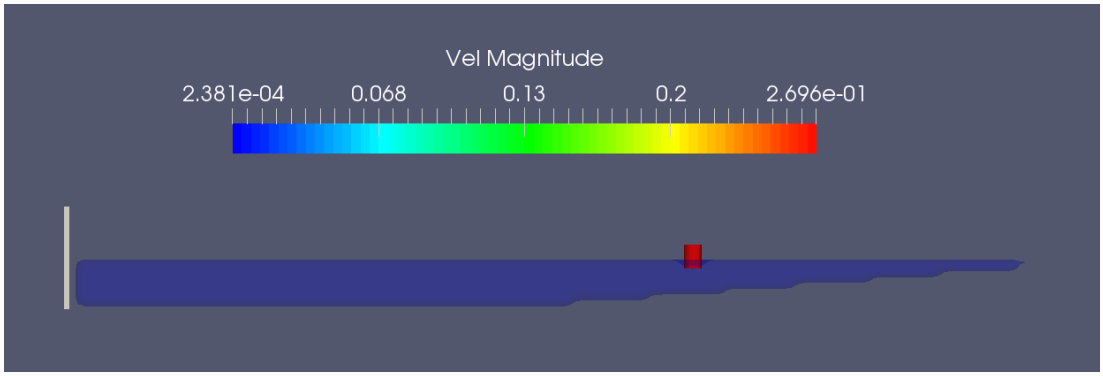

Figure 59 SPAR Platform at 0.14 M Water Depth at Time = 0.0 sec

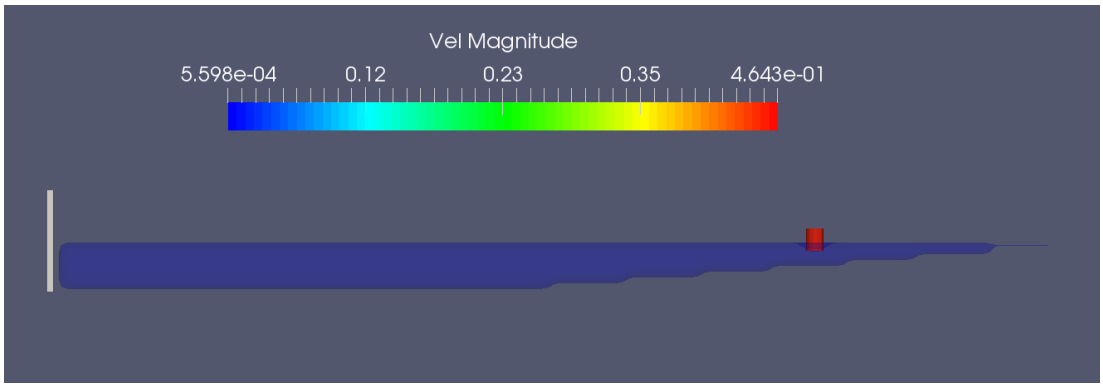

Figure 60 SPAR Platform at 0.1 M Water Depth at Time = 0.0 sec

Figure 57 shows the 3 reference lines used in this simulation. The 3 different initial positions of the SPAR correspond to varying water depths of 0.10 m, 0.14 m and 0.18 m.

The table below shows the parameters corresponding to their reference line.

Table 2 Reference Line Corresponding to Water Depth

Reference Line D1	Reference Line D2	Reference Line D3
0.10 m Water Depth	0.14 m Water Depth	0.18 m Water Depth

The following parameters are fixed while varying water depth:

- Wave Amplitude (V = 40 deg)
- Wave Frequency (1.0 waves/sec)

The simulation is run and the angular pitch of the SPAR with respect to time is plotted graphically.

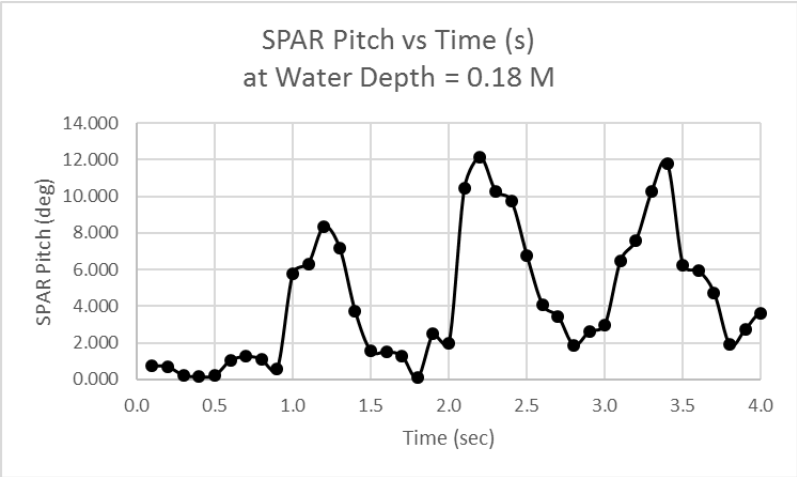

Figure 61 SPAR Pitch vs Time at Water Depth 0.18 m (D3)

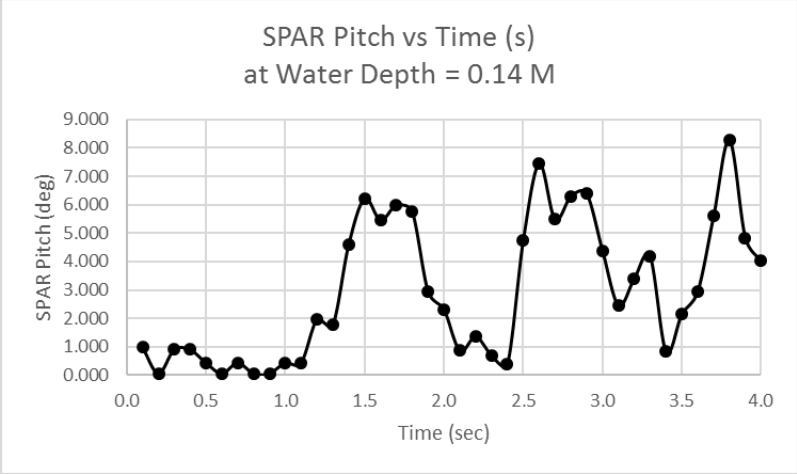

Figure 62 SPAR Pitch vs Time at Water Depth 0.14 m (D2)

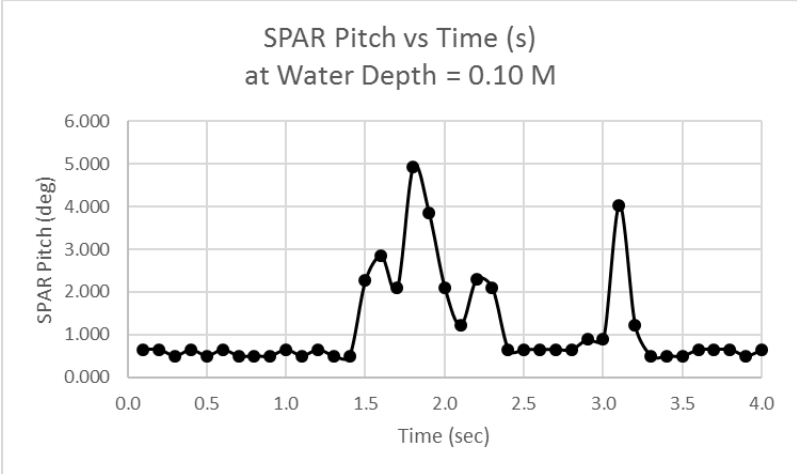

Figure 63 SPAR Pitch vs Time at Water Depth 0.10 m (D1)

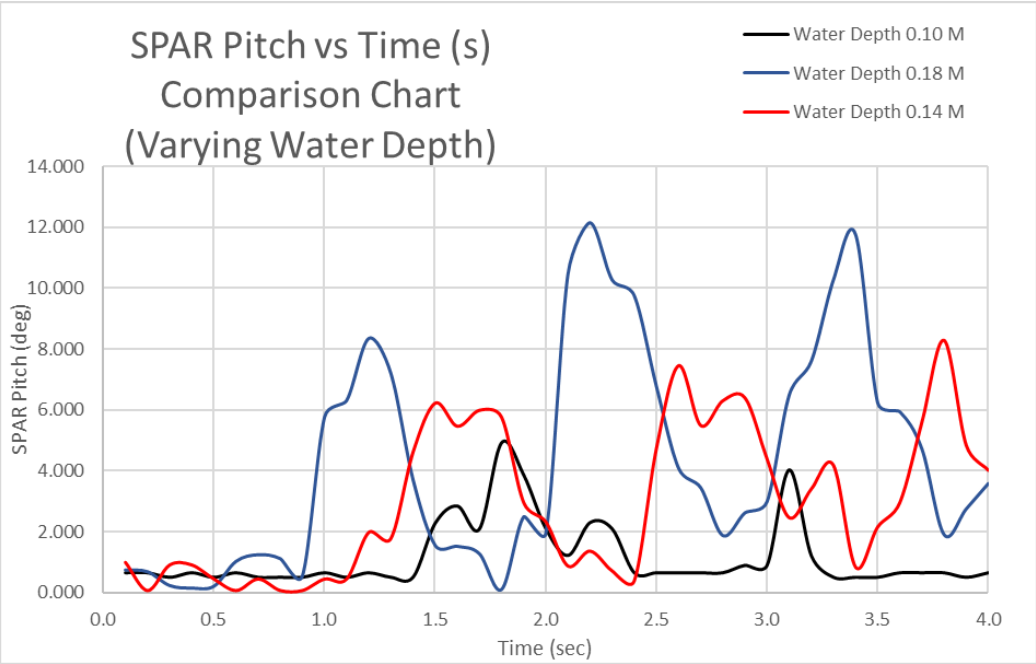

Figure 64 Comparison between Pitch of SPAR at Different Water Depths

In **Figure 61**, at 0.18 m water depth, it can be seen that that the maximum angular pitch achieved is about 12 degrees. In **Figure 62**, at 0.14 m water depth, the maximum angular pitch achieved is 8 degrees. Last but not least, in **Figure 63**, at 0.10 m water depth, the maximum angular pitch is 5 degrees.

It can also be observed that the SPAR performs at a more stable rate when in shallower waters. As can be seen in **Figure 64**, the fluctuations of the angular pitch of the SPAR is much more significant at higher water depths. This is due to the extra energy that the wave transmits at deeper waters.

Based on **Figures 61 – 64**, it can be observed that a greater water depth actually increases the angular pitch of the SPAR Platform. Based on these results, it can be concluded that maximum angular pitch of the SPAR is directly proportional to the water depth.

4.4 Effect of Varying Wave Frequency on Angular Pitch of SPAR

In this study, the angular pitch of the SPAR is studied while varying the wave frequency. The wave frequency of the waves is varied based on the table below:

Table 3 Wave Frequency Variations

Wave Frequency 1	Wave Frequency 2	Wave Frequency 3
1.0 waves/sec	1.5 waves/sec	2.0 waves/sec

The initial position of the SPAR is as shown in the figure below:

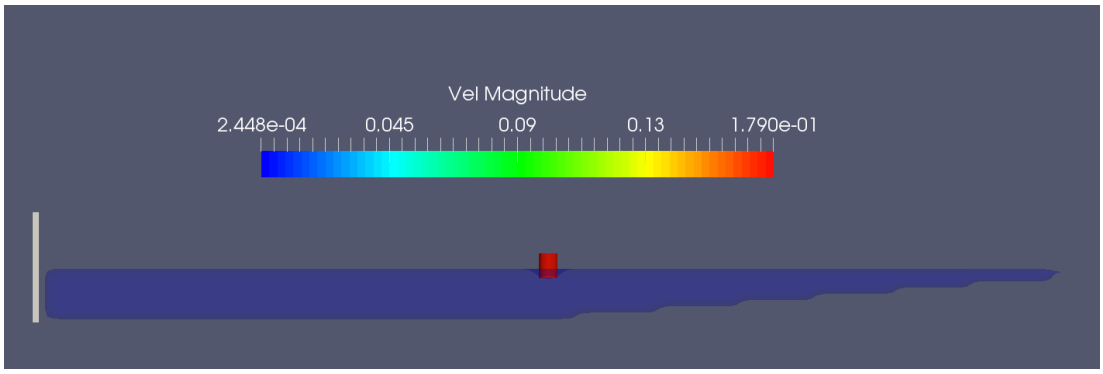

Figure 65 Initial Position of the SPAR

The following parameters are fixed while varying wave frequency:

- Wave Amplitude (V = 40 deg)
- Water Depth (0.18 m)

The simulation is run and the angular pitch of the SPAR with respect to time is plotted graphically.

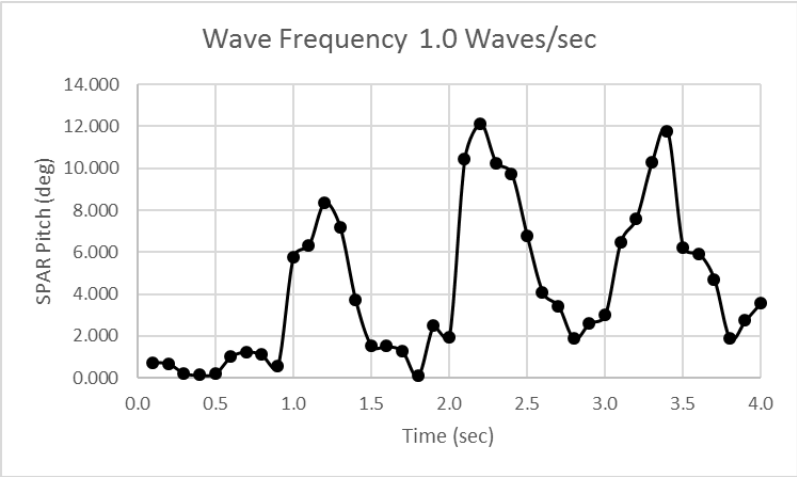

Figure 66 SPAR Pitch vs Time at Wave Frequency 1.0 waves/sec

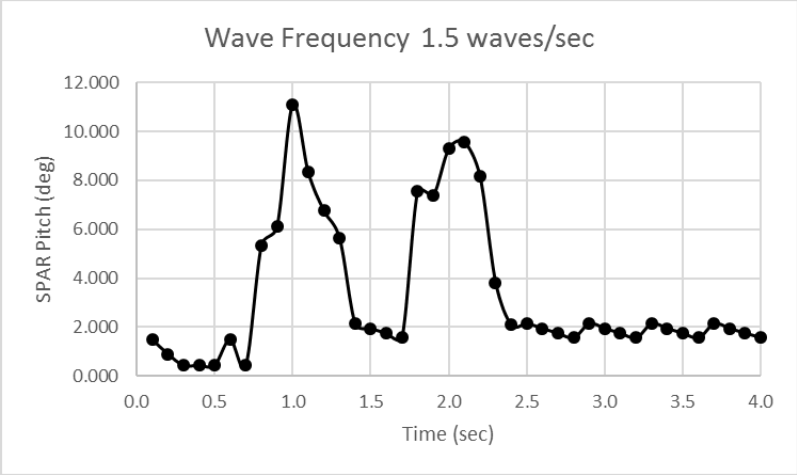

Figure 67 SPAR Pitch vs Time at Wave Frequency 1.5 waves/sec

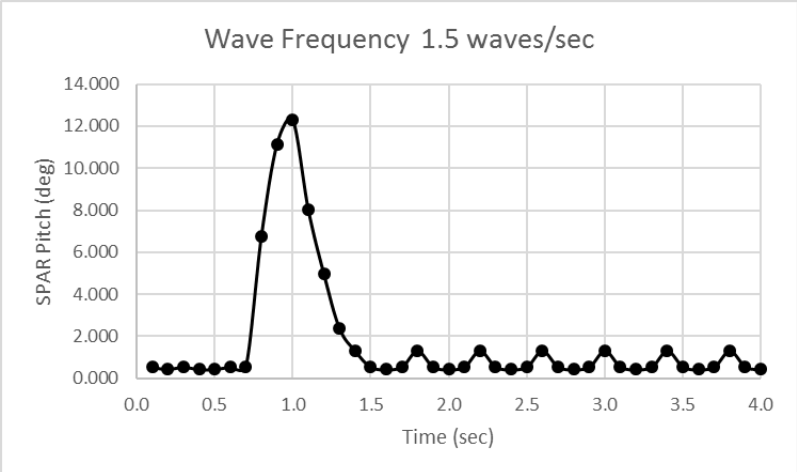

Figure 68 SPAR Pitch vs Time at Wave Frequency 2.0 waves/sec

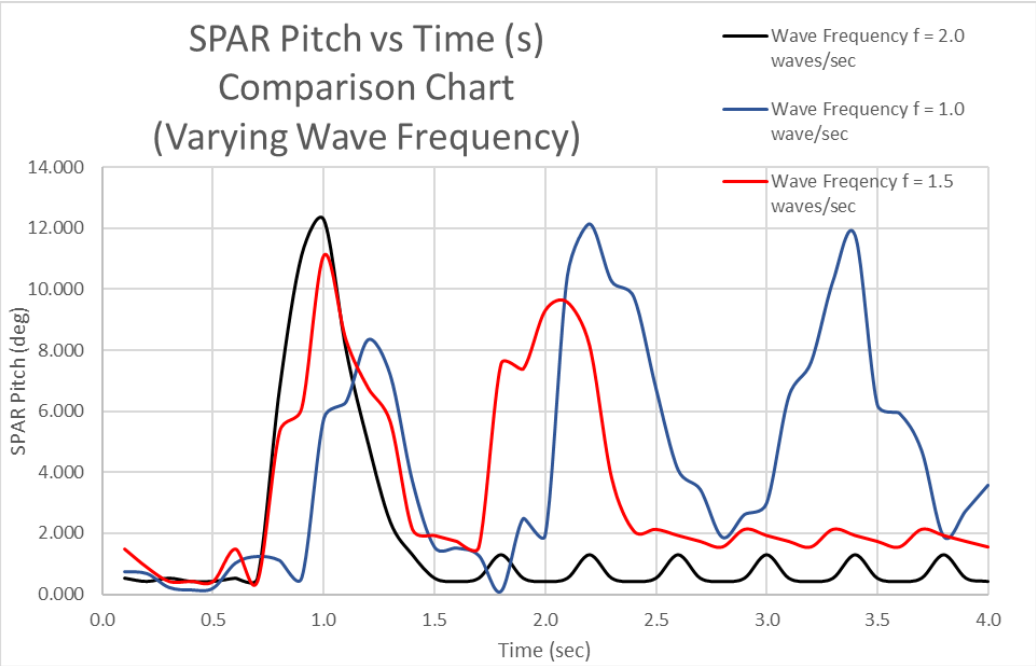

Figure 69 Comparison between Pitch of SPAR at Different Wave Frequencies

In **Figure 66**, the maximum angular pitch at 1.0 waves/sec is 12 degrees. In **Figure 67**, at 1.5 waves/sec, the maximum angular pitch is 11 degrees. **In Figure 68**, at 2.0 waves/sec, the maximum angular pitch is 12 degrees. This observation shows that the wave frequency does not have a significant effect on the angular pitch of the SPAR.

However, it can be observed from **Figure 69**, that as the wave frequency is increased, the peaks of angular pitch actually decreases with increasing wave frequency. This can be due to the faster speed of the piston-flap that contributes to a lower contact time with the fluid that causes it to be unable to scoop up more fluid as the fluid has not enough time to flow back towards the piston-flap.

4.5 Effect of Varying Wave Amplitude on Angular Pitch of SPAR

In this study, the angular pitch of the SPAR is studied while varying the wave amplitude. The wave amplitude of the waves is varied based on the table below:

Table 4 Wave Amplitude Variations

Wave Amplitude 1	Wave Amplitude 2	Wave Amplitude 3
V = 20 degrees	V = 30 degrees	V = 40 degrees

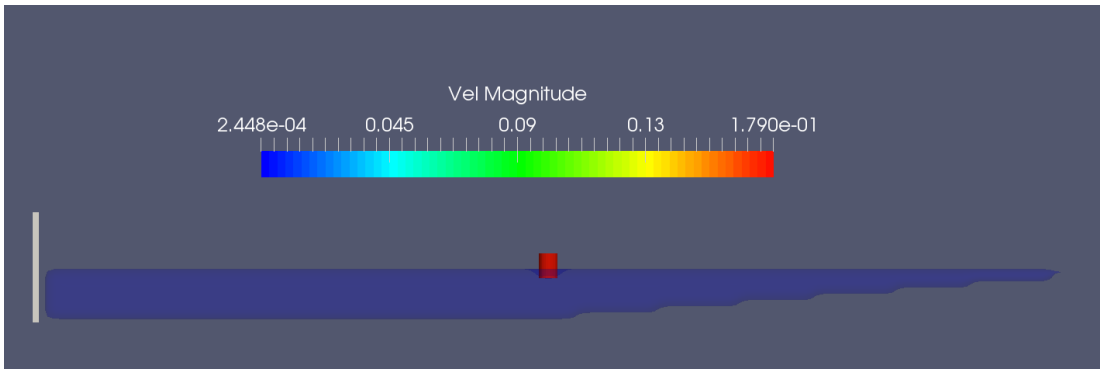

Figure 70 Initial Position of SPAR at all Wave Amplitudes

The following parameters are fixed while varying wave frequency:

- Wave Frequency (f = 1.0 waves/sec)
- Water Depth (0.18 m)

The simulation is run and the angular pitch of the SPAR with respect to time is plotted graphically.

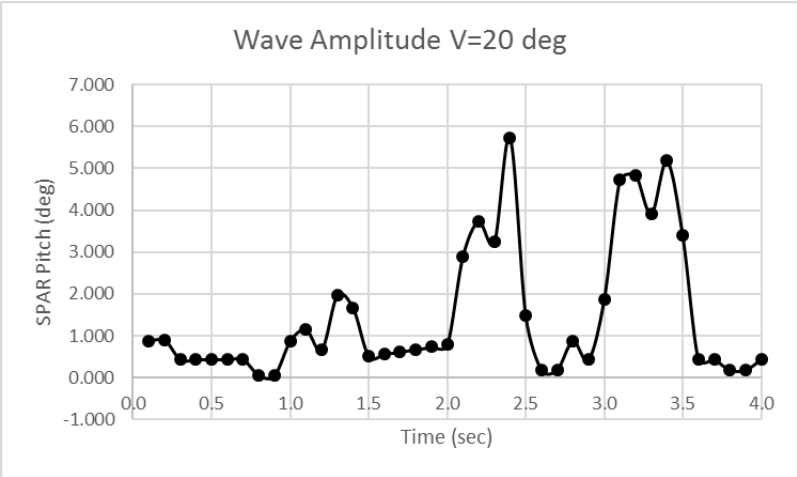

Figure 71 SPAR Pitch vs Time at Wave Amplitude V = 20 degrees

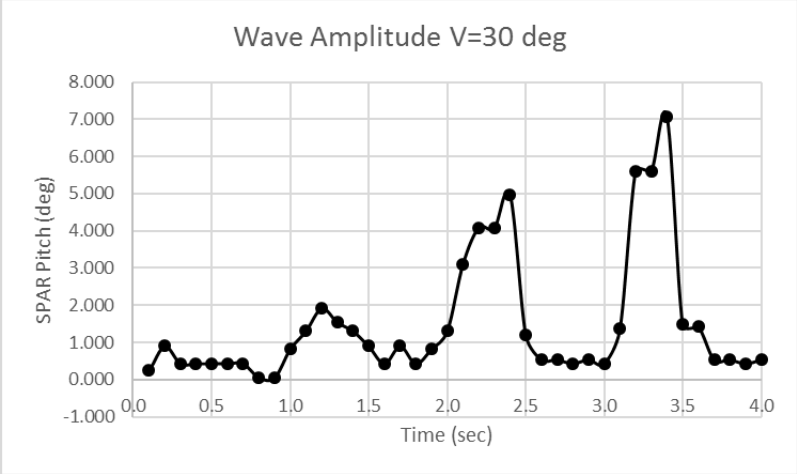

Figure 72 SPAR Pitch vs Time at Wave Amplitude V = 30 degrees

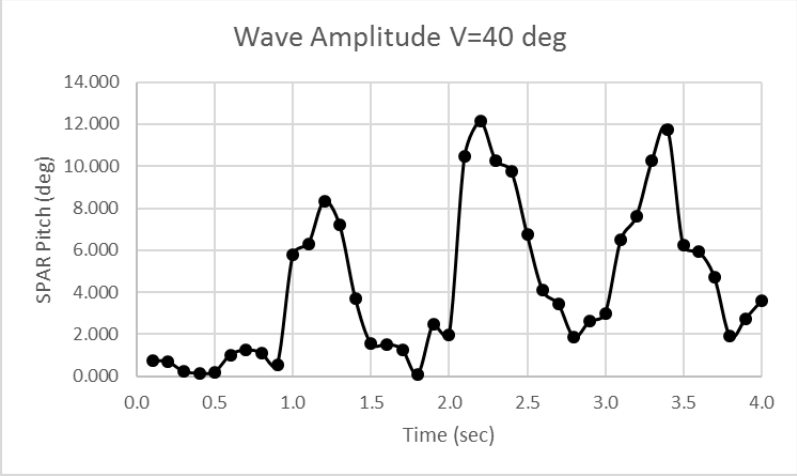

Figure 73 SPAR Pitch vs Time at Wave Amplitude V = 40 degrees

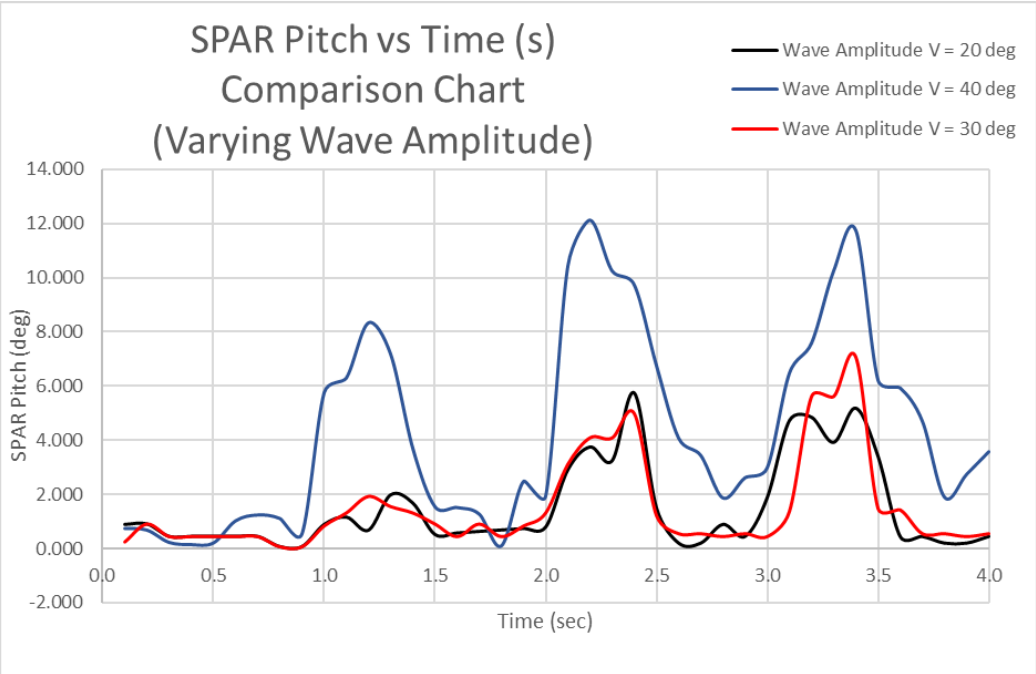

Figure 74 Comparison between Pitch of SPAR at Different Wave Amplitudes

In **Figure 71**, the maximum angular pitch at wave amplitude 20 degrees is 6 degrees. In **Figure 72**, the maximum angular pitch at wave amplitude of 30 degrees is 7 degrees. In **Figure 73**, the maximum angular pitch at wave amplitude of 40 degrees is 12 degrees.

By comparing all three charts in **Figure 74**, it can be observed that the angular pitch of the SPAR is significantly lower at smaller wave amplitudes. Therefore, it can be concluded that the angular pitch of the SPAR is directly proportional to the wave amplitude. This could be due to the fact that the smaller wave amplitude carries less initial energy and there is less significant energy that can actually affect the SPAR due to propagation losses.

Chapter 5

Conclusions & Recommendations

5.1 Conclusions

In this project, it has been conclusively proven that the behavior of deep-water SPAR Platforms can be simulated using the Smoothed Particle Hydrodynamics method rather accurately with low errors. The various validations carried out on Dam Break flows shows that the SPH method has a promising use for simulating extreme waves. In this study, after conducting numerical studies on the angular pitch of the SPAR when subjected to different wave conditions, various conclusions can be drawn. First, it can be concluded that the maximum angular pitch of the SPAR is directly proportional to the water depth. Second, the maximum angular pitch is directly proportional to the wave amplitude. Last but not least, the wave frequency does not significantly affect the angular pitch of the SPAR while increasing the wave frequency actually decreases the peaks of maximum angular pitch.

5.2 Recommendations

1. Research can be done on green-water loading and its effects on SPAR Platforms by coupling the SPH method with finite element analysis. This research shall be useful in simulating larger and more complex structures.
2. Research should be done on the responses of more complex structures such as Semi-submersibles. This could be extremely useful to offshore drilling rig constructors.

References

Buchner, B., & Bunnik, T. (2007). *Extreme Wave Effects on Deepwater Floating Structures*.

Campbell, J., Vignjevic, R., & Patel, M. H. (2008). *A Coupled FE-SPH pproach for Simulation of Structural Response to Extreme Wave and Green Water Loading*.

Cao, H., & Wan, D. (2012). *Numerical Investigation of Extreme Wave Effects On Cylindrical Offshore Structures*.

De Chowdhury, S., & Sannasiraj, S. (2013). *Numerical simulation of 2D wave impact pressure using SPH schemes.* Paper presented at the The Twenty-third International Offshore and Polar Engineering Conference.

Gingold, R. A., & Monaghan, J. J. (1977). Smoothed particle hydrodynamics: theory and application to non-spherical stars. *Monthly notices of the royal astronomical society, 181*(3), 375-389.

Guilcher, P. M., Couty, N., Brosset, L., & Le Touzé, D. (2012). *Simulations of Breaking Wave Impacts On a Rigid Wall At Two Different Scales With a Two Phase Fluid Compressible SPH Model*.

Haselton, F. R. (1976). Semi-submersible vessels: Google Patents.

Islam, A. S., Jameel, M., Jumaat, M. Z., Shirazi, S., & Salman, F. A. (2012). Review of offshore energy in Malaysia and floating Spar platform for sustainable exploration. *Renewable and Sustainable Energy Reviews, 16*(8), 6268-6284.

Jian, W., Liang, D., & Shao, S. (2011). *Simulation of Solitary Wave Impact On Coastal Structures Using Weakly Compressible And Incompressible SPH Methods*.

Karsan, D. I., Valdivieso, J. B., & Suhendra, R. (1986). *An Economic Study On Parameters Influencing The Cost Of Deepwater Fixed Platforms*.

Knowles, N., Selwa, J. R., & Bankes, G. J. (1999). *FPSOs Lessons Learned*.

Koshizuka, S., & Oka, Y. (1996). Moving-particle semi-implicit method for fragmentation of incompressible fluid. *Nuclear science and engineering, 123*(3), 421-434.

Lubeena, R., & Gupta, V. (2013). *Hydrodynamic Wave Loading on Offshore Structures*.

Ma, Q. W., Yan, S., Zhou, J., Duan, W. Y., & Zheng, X. (2009). *Numerical Study On Impact Pressure Due to Violent Sloshing Waves*.

Mastrangelo, C. F., & Henriques, C. C. D. (2000). *Petrobras Experience On the Operation of FPSOs*.

Narold, R., Willemse, O., & Brenninkmeijer, C. *SS: Spar Technology- Developments in Deepwater spar installation*.

Ozmen-Cagatay, H., & Kocaman, S. (2011). Dam-break flow in the presence of obstacle: experiment and CFD simulation. *Engineering applications of computational fluid mechanics, 5*(4), 541-552.

Pablo A. Caron, M. A. C., Axel E. Larretguy. (2015). Sensitivity analysis of finite volume simulations of a breaking dam problem. *International Journal of Numerical Methods for Heat & Fluid Flow*.

Rudman, M., & Cleary, P. W. (2009). *Oblique Impact of Rogue Waves On a Floating Platform*.

Thilleul, O., Drouet, A., Andrillon, Y., Guilcher, P. M., Jacquin, E., Barcarolo, D., . . . Legregeois, N. (2015). *CFD tools and adapted methodologies for Marine and Offshore Engineering projects*.

Wang, Y. (1996). *Wave Slamming On Offshore Structure*.